AD-A032 851 HONEYWELL RADIATION CENTER LEXINGTON MASS F/G 17/5
10.6-MICRON (HG,CD)TE PHOTODIODE MODULE.(U)
OCT 76 T KOEHLER DAAB07-71-C-0236
UNCLASSIFIED ECOM-71-0236-F NL

| OF |
AD
A032851

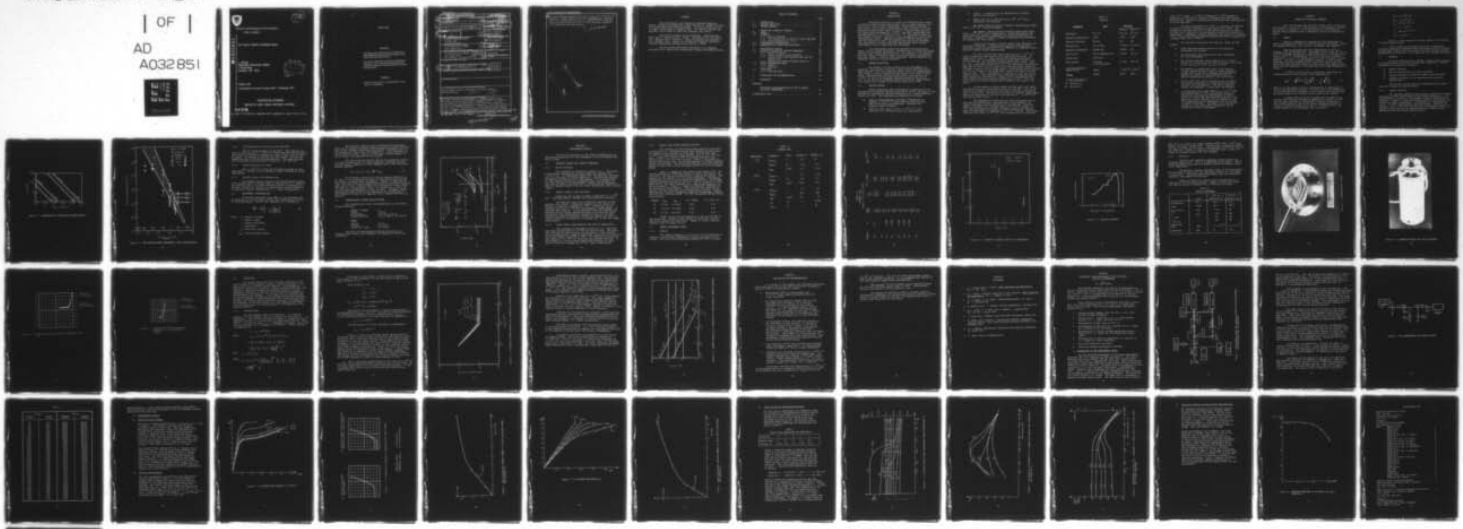

END

DATE
FILMED
1-77

Research and Development Technical Report

ECOM-71-0236-F

10.6 Micron (HgCd)Te Photodiode Module

T. Koehler
HONEYWELL RADIATION CENTER
2 Forbes Road
Lexington, MA 02173

October 1976

Final Report for Period 15 August 1974 - 15 December 1975

DISTRIBUTION STATEMENT

Approved for public release; distribution unlimited.

ECOM

US ARMY ELECTRONICS COMMAND FORT MONMOUTH, NEW JERSEY 07703

NOTICES

Disclaimers

The findings in this report are not to be construed as an official Department of the Army position, unless so designated by other authorized documents.

The citation of trade names and names of manufacturers in this report is not to be construed as official Government indorsement or approval of commercial products or services referenced herein.

Disposition

Destroy this report when it is no longer needed. Do not return it to the originator.

UNCLASSIFIED

SECURITY CLASSIFICATION OF THIS PAGE (When Data Entered)

REPORT DOCUMENTATION PAGE

READ INSTRUCTIONS BEFORE COMPLETING FORM

1. REPORT NUMBER: ECOM-71-0236-F	2. GOVT ACCESSION NO.
3. RECIPIENT'S CATALOG NUMBER: (Rept.)	
4. TITLE (and Subtitle): 10.6-MICRON (Hg,Cd)Te PHOTODIODE MODULE.	5. TYPE OF REPORT & PERIOD COVERED: Final 15 Aug 1974 - 15 Dec 1975
	6. PERFORMING ORG. REPORT NUMBER
7. AUTHOR(s): Irving J. Koehler	8. CONTRACT OR GRANT NUMBER(s): DAAB07-71-C-0236
9. PERFORMING ORGANIZATION NAME AND ADDRESS: Honeywell Radiation Center, 2 Forbes Road, Lexington, MA 02173	10. PROGRAM ELEMENT, PROJECT, TASK AREA & WORK UNIT NUMBERS: 1S7 62703 DH93D1033
11. CONTROLLING OFFICE NAME AND ADDRESS: US Army Electronics Command, Attn: AMSEL-CT-L-C, Fort Monmouth, New Jersey 07703	12. REPORT DATE: October 1976
	13. NUMBER OF PAGES: 51
14. MONITORING AGENCY NAME & ADDRESS (if different from Controlling Office): US Army Electronics Command, Attn: AMSEL-CT-L-C, Fort Monmouth, New Jersey 07703 (12) 53p.	15. SECURITY CLASS. (of this report): UNCLASSIFIED
	15a. DECLASSIFICATION/DOWNGRADING SCHEDULE

16. DISTRIBUTION STATEMENT (of this Report)

~~Approved for Public Release; Distribution Unlimited~~

(16) 1S762703DH93 (17) D1

17. DISTRIBUTION STATEMENT (of the abstract entered in Block 20, if different from Report)

18. SUPPLEMENTARY NOTES

19. KEY WORDS (Continue on reverse side if necessary and identify by block number)

Mercury Cadmium Telluride; Photodiode; 10.6 Micron Detector; Heterodyne Detector

20. ABSTRACT (Continue on reverse side if necessary and identify by block number)

This report describes the development of a 10.6-μm (Hg,Cd)Te thermoelectrically cooled photodiode module operating at 174 K. The objective of the program was the demonstration of 170 K operation with quantum efficiency of 20 percent, bandwidth of 50 MHz and a 1 mA reverse saturation current in a 5×10^{-4} cm^2 area device. Several approaches were assessed in order to achieve a heavily doped junction that would minimize diffusion current at 170 K. Two 10.6-μm (Hg,Cd)Te Photodiode Modules, each consisting

DD FORM 1 JAN 73 1473 EDITION OF 1 NOV 65 IS OBSOLETE

UNCLASSIFIED

SECURITY CLASSIFICATION OF THIS PAGE (When Data Entered)

404486

.0002 Ω-cm.

20.

of a n-on-p diffused (Hg,Cd)Te diode with an active area of 2×10^{-4} cm^2 mounted on a 6-stage thermoelectric cooler, were delivered. The better device had a minimum detectable power of 7.7×10^{-11} W/Hz, 23 MHz bandwidth, and 8.8 mA saturation current at 174 K. The power consumption for the module was less than 20 watts.

10 to the -19th power

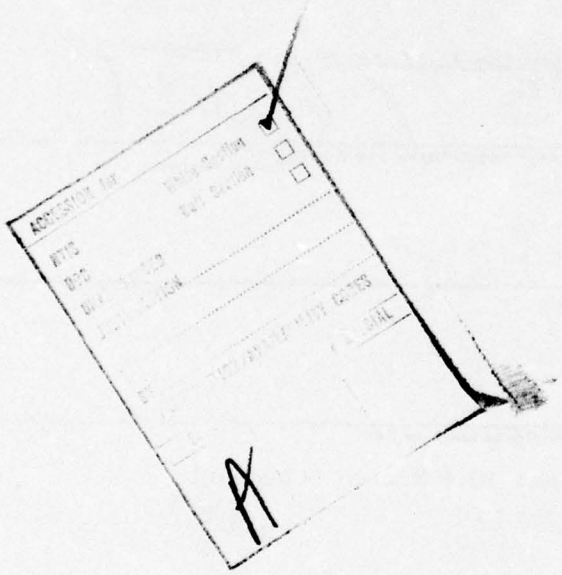

PREFACE

This Final Report was prepared by Honeywell Radiation Center, Lexington, Massachusetts, under Contract No. DAAB07-71-C-0236, 10.6 Micron (Hg,Cd)Te Photodiode Module. It covers the period from 15 August 1974 through 15 December 1975. The Contract Monitor has been Mrs. Claire Burke at ECOM, Fort Monmouth, New Jersey.

The Project Engineer was Toivo Koehler. Materials Engineers were R. Lancaster and B. Jindal. The devices were fabricated by L. Gauthier and J. Faticanti. Device evaluation was performed by R. Bechdolt and R. Healey, and theoretical computer modeling of elevated temperature performance was done by S. Tobin.

The heterodyne measurements described in the Appendix were made by Dr. Hans Mocker of Honeywell Systems and Research Center.

TABLE OF CONTENTS

SECTION 1

INTRODUCTION

Heterodyne detection as a means for detecting weak signals is useful in many systems applications, such as remote sensing, communications, optical radar rangefinders, battlefield surveillance and velocity and turbulence measurements. The technique is not new; minimum detectable power (MDP) of 7×10^{-20} W/Hz has been reported for copper doped germanium at 4.2°K[1]. (Hg,Cd)Te photodiodes have achieved MDP of 8×10^{-20} W/Hz at 77°K[2,3]. The previous phase of this program reported a (Hg,Cd)Te 10.6-μm photomixer on a nine-stage thermoelectric cooler. Quantum efficiency or MDP has always been near the theoretical limit, but progress has occurred by extending this performance to higher operating temperatures where cooling requirements could be simplified for the system.

This development program has addressed several critical areas, such as quantum efficiency, leakage current at 170°K and thermoelectric cooler module miniaturization. The success of this development will have a significant impact on the development of practical CO_2 laser systems. Other critical components, such as miniature CO_2 waveguide lasers are already available.

1.1 PROGRAM OBJECTIVES

The objective of this program was the development of a practical, fast response sensitive, reverse biased (Hg,Cd)Te photodiode detector for 10.6-μm radiation which utilizes a thermoelectric (TE) cooler to reach an operating temperature in the 145°K to 190°K range. The photodiode detector with an active area greater than 5×10^{-4} cm^2 was to have quantum efficiency greater than 20% at 10.6 μm, an electrical bandwidth greater than 50 MHz, and a maximum 1-mA reverse bias leakage current while operating at 170°K.

1.2 PROGRAM SUMMARY

Several approaches were investigated in achieving 10.6-μm photodiodes with minimum saturation current at 170°K. The goal of each approach was to maximize junction doping and thus, reduce diffusion current at 170°K. The approaches are summarized as follows:

- Ingot or wafer quenched from higher temperatures to produce 3×10^{18} cm^{-3} p-type material resulting from high native defect concentration. Junctions are formed by donor diffusion.
- Impurity doped ingot to form 3×10^{18} cm^{-3} p-type. Junctions to be formed by donor ion implantation.

- Form p^+ - n junctions by ion implantation on heavily doped n-type material.
- Reduce area of n-p junctions on 1 x 10^{17} cm^{-3} defect dominated p-type material.

The quench approach failed to produce concentrations higher than 5 x 10^{17} cm^{-3} and was abandoned.

The impurity doping approach produced copper doped ingots with 3 x 10^{18} cm^{-3} p-type concentration. Indium implantation and indium diffusion failed to compensate the acceptors and form n-p junctions. Solubility limits of indium in (Hg,Cd)Te were considered as a problem for this process.

Implantation of gold on heavily doped n-type (Hg,Cd)Te did not produce junctions. Problems were associated with the rapid diffusion of gold in (Hg,Cd)Te and the inability to compensate donors after the implant damage removal anneal.

The final devices were fabricated from the 1 x 10^{17} cm^{-3} defect dominated p-type material with reduced junction area. As summarized in Table 1.1, these devices had quantum efficiencies greater than 20%. The minimum detectable power (MDP) of unit 1 was 7.7 x 10^{-19} W/Hz when operating in heterodyne mode at 170°K. This unit had a saturation current of 8.8 mA. Our theoretical calculations show that for these kind of diodes the saturation current cannot be reduced by much for the following reason: the diffusion current density at 170°K is limited by the n-side Auger lifetime and cannot be lower than 10 A/cm^2. This is equivalent to a current of 5 mA in a 250 μm diameter device. The consequence of a high dark current was high dc power dissipation resulting in a thermal load on the thermoelectric cooler which raised the operating temperature to 174°K. Also, the local oscillator induced current did not dominate the noise of the device.

An improvement in device design and fabrication can reduce the saturation current which would result in lower MDP. This can be achieved by reducing the detector area and by increasing the doping level of the p-side. The ability to control the impurity levels would enable the fabrication on n-p+ or n-pp+ devices (p+ > 1 x 10^{18} cm^{-3}) with smaller dark current.

The bandwidth of 23 MHz was less than anticipated from RC time constant calculations, and therefore, it was assumed to be limited by minority carrier diffusion to the junction. This bandwidth is equivalent to a response time of 6.91 x 10^{-9} seconds. At 170°K the n-side minority carrier lifetime is limited by intrinsic Auger lifetime which is calculated as 4.8 x 10^{-8} seconds. The p-side radiative limit with 6 x 10^{16} cm^{-3} hole concentration is calculated

Table 1.1

RESULTS

Parameter	Goal	Achieved	
		Unit 1**	Unit 2***
Wavelength	10.6 μm	10.6 μm	10.6 μm
Operating Temperature	170°K	174°K	174°K
Quantum Efficiency	20% min	21%	32%
Responsivity	1.6 A/W min	1.79 A/W	2.72 A/W
Electrical Bandwidth	50 MHz min	23 MHz	N/A
Active Area	250 μm Diameter min	150 μm	150 μm
Capacitance	20 pF max	*	*
Dark Current	3 mA max (1 mA desirable)	8.8 mA	10.5 mA
Minimum Detectable Power (W/Hz)	(None)	7.7×10^{-19}	4.0×10^{-17}
R_{SHUNT}	(None)	800 Ω	600 Ω

* Not measurable

** Detector F1

*** Detector G1

5.56×10^{-7} seconds. At $77^{o}K$ a lifetime of 1×10^{-9} seconds is measured in p-type and is limited by a Schockly-Read type recombination center. Radiative recombination rates have never been observed in p-type (Hg,Cd)Te.

The observed bandwidth of 23 MHz is, therefore, determined by minority carrier diffusion in p-type (Hg,Cd)Te at $170^{o}K$. The increase in lifetime from $77^{o}K$ to $170^{o}K$ can be explained by shifts in Fermi level relative to the recombination center as a function of temperature. Independent evidence supporting the increase of lifetime is the increase of diffusion-limited quantum efficiency as temperature increases from $77^{o}K$ to $170^{o}K$[4].

The following conclusions were made as a result of this program:

- $170^{o}K$ thermoelectrically-cooled 10.6-μm (Hg,Cd)Te photomixers are feasible.
- New performance and design limits were established for those photomixers.
- The minimum diffusion current density in the present devices is determined by the Auger lifetime of the n-side of the junction at $170^{o}K$ and it is 10 A/cm^2.
- The approach of doping the p-side of the junction to high concentrations in order to reduce diffusion current density was valid although the technique of quenching in defects to accomplish this did not achieve concentrations above 5×10^{17} cm^{-3} p-type.
- The 10 A/cm^2 limit can be achieved either by doping the p-side more heavily or increasing the electron lifetime in p-type material. The latter approach reduces the bandwidth, a result which was observed.
- A minimum detectable power (MDP) of 7.7×10^{-19} W/Hz was demonstrated at $174^{o}K$ in heterodyne operation. Calculations indicate that MDP degrades by only a factor of 3 with 5 mW total power dissipation if the saturation current density is 10 mA instead of 1 mA. This degradation can be compensated with an increase in quantum efficiency. The impact of an increase in current is on TE cooler power consumption and not necessarily detector performance.

SECTION 2

THEORY AND TECHNICAL APPROACH

This section describes the basic device theory of (Hg,Cd)Te photodiodes as it existed at the beginning of this program and how it was utilized to design a 10.6-μm photomixer for 170°K operation. Several unique approaches were attempted to realize the design parameters.

2.1 THEORY

Several parameters are important for the achievement of useful performance at 170°K in a 10.6-μm (Hg,Cd)Te photomixer. These are quantum efficiency, dark current, wavelength, and bandwidth.

Quantum efficiency has been demonstrated at 170°K by Koehler, Burke and McNally[4,6]. Wavelength can be tuned for 10.6 μm at 170°K by selecting (Hg,Cd)Te with composition of 0.194 mole fraction of CdTe[4,6]. Bandwidth at 77°K is RC limited or diffusion limited by a 1×10^{-9} in second minority carrier lifetime in p-type material. The most critical parameter, however, is dark current, which would introduce excessive shot noise and require high local oscillator power and which would introduce power dissipation levels which could be impossible to overcome with a six-stage thermoelectric cooler.

At 170°K the dark current is diffusion limited and the saturation value of this current can be expressed as:

$$J_{SAT} = -\sqrt{kTq}\, n_i^2 \left(\frac{1}{N_A} \sqrt{\frac{\mu_e}{\tau_e}} + \frac{1}{N_D} \sqrt{\frac{\mu_h}{\tau_h}} \right) \qquad (1)$$

where n_i is the intrinsic carrier concentration at temperature T and k is the Boltzmann constant. The first term in the parenthesis is the contribution of electrons in the p-side of the junction and the second term is due to holes in the n-side of the junction.

A simple model would be to assume that the mobility to lifetime ratio remains constant as temperature increases to 170°K and also that the ratio is independent of doping concentration. Such a model predicts that we can achieve saturation current of 2 A/cm^2 at 170°K by doping the p-side to 3×10^{18} cm^{-3}.[4] The values assumed for the parameters were as follows:

$$N_A = 3 \times 10^{18} \text{ cm}^{-3}$$

$$N_D = 1 \times 10^{16} \text{ cm}^{-3}$$

$$\mu_e = 10^5 \text{ cm}^2 \text{ V}^{-1} \text{ s}^{-1}$$

$$\tau_e = 1.0 \times 10^{-9} \text{ s}$$

$$\mu_h = 200 \text{ cm}^2 \text{ V}^{-1} \text{ s}^{-1}$$

$$\tau_h = 5 \times 10^{-7} \text{ s}$$

Figure 2.1 shows saturation current density as a function of carrier concentration.

A better model was developed during the program which introduced temperature dependent mobilities based on lattice scattering and Auger lifetime for the n-side of the junction and radiative recombination on the p-side. This model will be discussed in Section 3.

2.2 APPROACH

The basic approach was to achieve a heavily doped junction in (Hg,Cd)Te having 0.194 mole fraction CdTe composition. Several approaches were assessed in sequence:

- Quench Technique.
- Gold ion implantation in n-type (Hg,Cd)Te.
- Indium diffusion into impurity doped p-type (Hg,Cd)Te
- Standard technique in low concentration p-type with reduced area

The two best devices from any technique would be candidates for integration with TE coolers.

2.2.1 Quench Technique

The (Hg,Cd)Te annealed under mercury pressure has a unique equilibrium p-type concentration at each anneal temperature. This concentration is related to stoichiometric defects which behave as acceptors. Figure 2.2 shows equilibrium acceptor concentration as a function of anneal temperature. In principle each concentration can be "frozen" in by quenching from the anneal. Therefore, to achieve P_o of 3×10^{18} cm^{-3} the wafer must be annealed at 600°C and quenched. The junctions are fabricated by the standard planar indium diffusion and mercury anneal process.

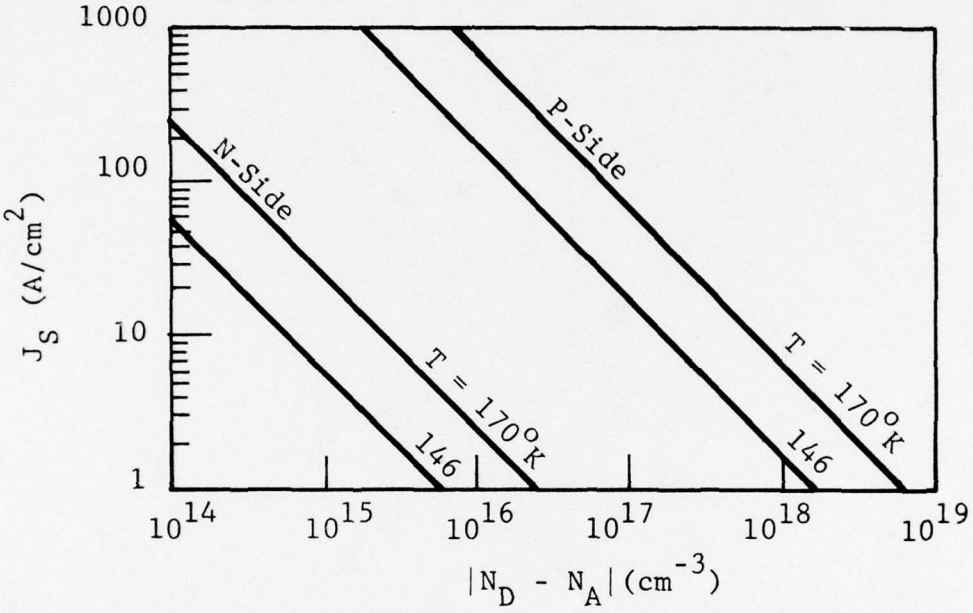

Figure 2.1 CONTRIBUTION TO SATURATION CURRENT DENSITY

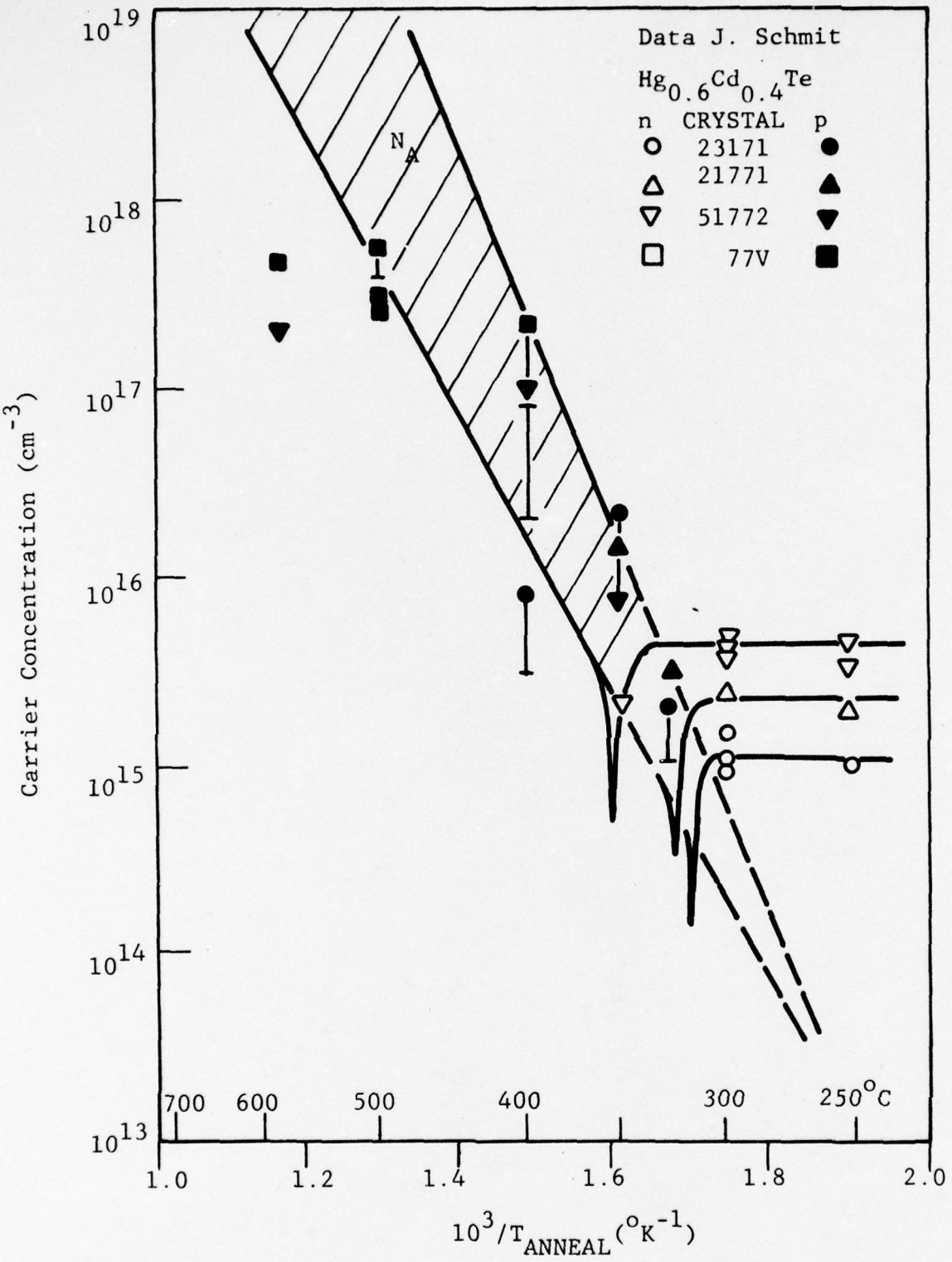

Figure 2.2 EQUILIBRIUM DEFECT DETERMINED P-TYPE CONCENTRATION

2.2.2 Ion Implantation of Gold in n-type (Hg,Cd)Te

Gold is a known acceptor in (Hg,Cd)Te. This approach consists of starting with 1.0×10^{16} cm-3 n-type (Hg,Cd)Te and implanting gold through a photoresist implantation mask to form a heavily doped p+ region. The implant is followed by a post-anneal; the time and temperature must be determined experimentally. The dose and energy can be calculated from LSS theory to give p+ of 3×10^{18} cm^{-3}.

2.2.3 Indium Diffusion in p-type

The 3×10^{18} cm^{-3} p-type will be grown by doping an ingot with copper. Junctions will be formed by indium diffusion or indium implantation.

2.2.4 Standard Process with Reduced Area

The standard process consists of indium diffusion through a ZnS diffusion mask in mercury vapor as described by D. L. Spears[8]. The objective here is to reduce diffusion current by reducing size and also consider the effects of p-side minority carrier lifetime as a function of carrier concentration; i.e., defect concentration.

2.3 PERFORMANCE CONSIDERATIONS

The minimum detectable power (MDP) in the heterodyne mode of operation is a useful figure of merit for evaluating the 10.6-μm TE cooled photomixer. MDP per unit bandwidth (B) is defined as:

$$\frac{MDP}{B} = \frac{hc}{\eta\lambda}\left[1 + \frac{I_s}{P_{LO}\left(\frac{q\lambda\eta}{hc}\right)}\right] \qquad (2)$$

where: h = Planck's constant

c = Speed of light

η = Quantum efficiency

λ = Wavelength

I_s = Saturation current

P_{LO} = Local oscillator power

This equation indicates that the theoretical performance limit can be achieved by either reducing saturation current (In which case we are ultimately amplifier noise limited. Amplifier noise is not included as a factor for 170°K operation.), or by increasing the local oscillator power. Because of the finite cooling capacity of the TE cooler, this approach is also limited.

The total power dissipation (P_D) in the photomixer consists of optical absorption and dc power dissipation resulting from bias (V_r) and current composed of a dark component and a local oscillator induced component:

$$P_D = P_{LO} + V_r \left(I_s + \frac{\eta \lambda q}{hc} P_{LO}\right) \qquad (3)$$

If we assume a bias of 0.2 volt and quantum efficiency of 0.2 and 0.5, we can examine the effect of saturation current on MDP for values of constant power dissipation. Figure 2.3 shows MDP for 3 mW, 5 mW, and 10 mW power dissipation levels for saturation currents from 1 mA to 10 mA. Five milliwatt power dissipation is well within the limit of a thermoelectric cooler. An increase in I_s from 1 mA to 10 mA would degrade MDP by a factor of three. Therefore, useful thermoelectrically cooled 10.6-μm photomixers can be made even if the saturation current is not improved, but if quantum efficiency is improved.

2.4 THERMOELECTRIC COOLER SPECIFICATIONS

The thermoelectric cooler was manufactured to the following specifications:

Number of Stages	6
Height	2.03 cm
Cold Surface	0.42 cm x 0.42 cm
Vacuum Enclosure	4.19 cm high x 6.35 cm dia
<u>Power</u>	
Current	3.6 A
Voltage	6.4 volts
Power (10^{-6} torr)	19.5 watts

The units are manufactured by Marlow Industries and include a power supply, heat exchanger and temperature monitoring thermistors.

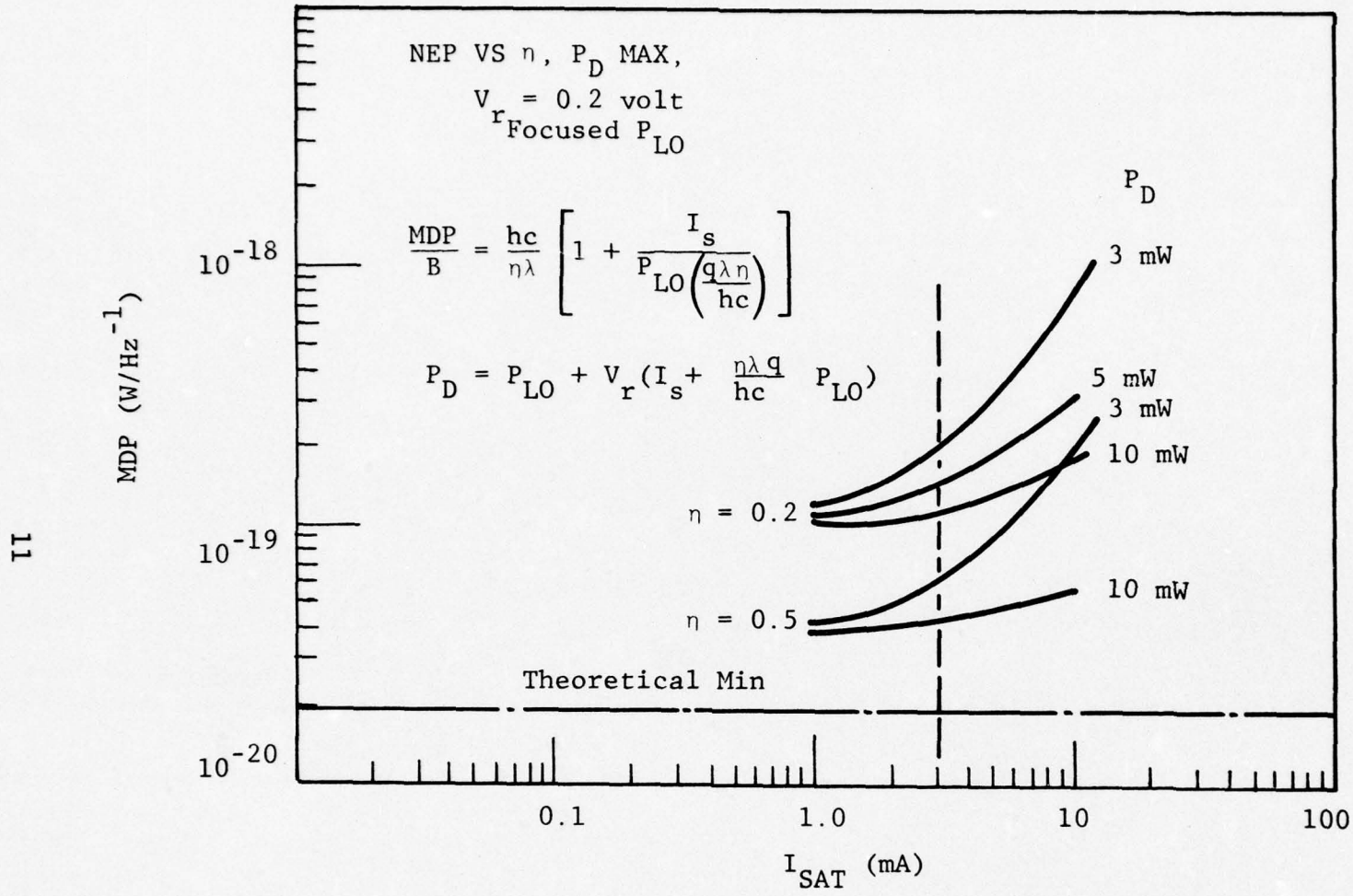

Figure 2.3 MDP VS SATURATION CURRENT

SECTION 3

EXPERIMENTAL RESULTS

This section describes (1) the results achieved with the approaches utilized and (2) the performance of the two modules delivered to ECOM.

3.1 MATERIALS GROWTH AND JUNCTION FORMATION

3.1.1 Quench Technique

This technique is described in Section 2.2.1. The highest p-type carrier concentration achieved with this technique was 5×10^{17} cm^{-3}. At temperatures above 450°C, the resultant concentration was independent of anneal temperature. Quenching was achieved by immersing the ampoule in oil and breaking. It is assumed that the time required to achieve equilibrium defect concentration is less than the quench time above 500°C. Diodes were not fabricated from this material since it did not differ significantly from as-grown ingots.

3.1.2 Impurity Doped p-type (Hg,Cd)Te

Copper was used to dope an ingot of (Hg,Cd)Te to 3×10^{18} cm^{-3}. Hall measurements indicate that this method was successful.

Two techniques were used to fabricate junctions in this material, both failed. Indium was evaporated on the surface and diffused in a mercury atmosphere at 275°C. Indium was also ion implanted (10^{15} cm^{-2} at 200 KeV) and annealed to remove damage. No junctions were observed. It was speculated that the diffusion temperature and post-anneal temperatures were too low and the indium concentration was determined by a solubility limit or the rapid diffusion of indium in (Hg,Cd)Te diffused the indium so it did not achieve sufficient concentration to overdope the 3×10^{18} cm^{-3} copper concentration.

3.1.3 Indium Doped n-type Material and Gold Ion Implantation

This technique is described in Section 2.2.2. (Hg,Cd)Te with donor concentration of 1×10^{16} cm^{-3} was selected. The indium donor had been introduced during crystal growth. A gold acceptor was ion implanted and a range of post-anneal conditions were evaluated with times ranging from 150°C to 275°C. No junctions were observed. Gold implants in 5×10^{14} cm^{-3} material have produced junctions. It was assumed that the post-anneal caused gold diffusion to levels where it could not overdope the 10^{16} cm^{-3} donor concentration.

3.1.4 Reduced Area Indium Diffused Junction

The technique for fabricating these devices is described in Section 2.2.4. Successful devices were achieved by this method. Two typical process batches are described. Process 3201 used 2×10^{17} cm^{-3} zone leveled p-type material and a 5×10^{-4} cm^2 area mask. Process 3233 used 6×10^{16} cm^{-3} quench annealed p-type material and a 1.8×10^{-4} cm^2 area mask. Table 3.1 describes two devices from Process 3201. The reverse impedance to forward impedance ratios are very high. The current densities are quite low and would produce a device with 3.6-mA saturation current in a 150-μm diameter device.

Table 3.2 summarizes some devices from Process 3233. The current densities at 146°K were higher in Process 3233 than in Process 3201. This may be associated with a lower p-side doping. Some devices did not achieve a 10.6-μm cutoff wavelength. The quantum efficiencies were good and increased with temperature. The optimum quantum efficiency occurred at 30 mV at 77°K and at 200 mV at 146°K. Below 200 mV, the device impedance was 5 ohms as determined by the series resistance. Figure 3.1 shows the temperature dependence of the saturation current density. These devices were selected from Process 3233 for integration with thermoelectric coolers. Current densities at 170°K were extrapolated from fixed measurement temperatures of 77°K, 146°K and 193°K. At 170°K the devices had the following properties.

Element	i_{SAT}	J_{SAT}	Q.E. (Peak)	Q.E. (10.6 μm)
E2	9.5 mA	52 A/cm^2	0.55	0.27
F1	6.75 mA	37 A/cm^2	0.427	0.21
G1	14.6 mA	80 A/cm^2	0.67	0.32

Element E2 was rejected because of a chip on the edge of the active area. Element F1 was mounted in cooler S/N 1 and element G1 was mounted in cooler S/N 2. Figure 3.2 shows a spectral response curve of element 3233 F1.

3.2 MODULE PERFORMANCE TESTS

3.2.1 Modules

The elements mounted in a 0.44 cm x 0.44 cm flatpack were cemented to the 6-stage thermoelectric cooler stock with GE 7031 varnish. The cooler and housing were prebaked at 105°C in vacuum.

Table 3.1
PROCESS 3201

Temperature	Parameter	Units	Element A1	Element A2
77°K	R_{series}	Ω	8.3	10
	R_{shunt}	KΩ	1.55	3.9
	J_{SAT}	A/cm^2	0.2	0.16
146°K	R_{series}	Ω	5.4	6.25
	R_{shunt}	KΩ	0.8	1.2
	J_{SAT}	A/cm^2	14.8	9.6
170°K	R_{series}	Ω	4.3	4.8
	R_{shunt}	Ω	550	600
	J_{SAT}	A/cm^2	26	18
	λ_{co}	μm	--	10.84
	$\eta_{10.6}$	%	--	14

Table 3.2

PROCESS 3233

(Area = 1.8×10^{-4} cm^2)

Element	X	Temp (^oK)	λ_{co} (μm)	Q.E. (peak) λ	J_{SAT} (A/cm^2)
D1	0.2	77	13.2	0.43	---
		146	10.76	0.59	9.32
		170	10.1		---
D2		77		0.47	---
		146		0.67	
E1	0.196	77	14.0	0.30	---
		146	11.3	--	15.9
E2	0.196	77	14.0	0.37	---
		146	11.3	0.65	21.9
		170	10.6		
F1	0.196	77	14.0	0.34	---
		146	11.3	0.42	17.0
F2	0.196	77	14.0	0.40	---
		146	11.3	0.68	32.9
G1	0.196	77	14.16	0.579	---
		146	11.4	0.673	36.0
		170	10.66	--	--
G2		77	--	0.30	---
		146	--	0.65	49.3

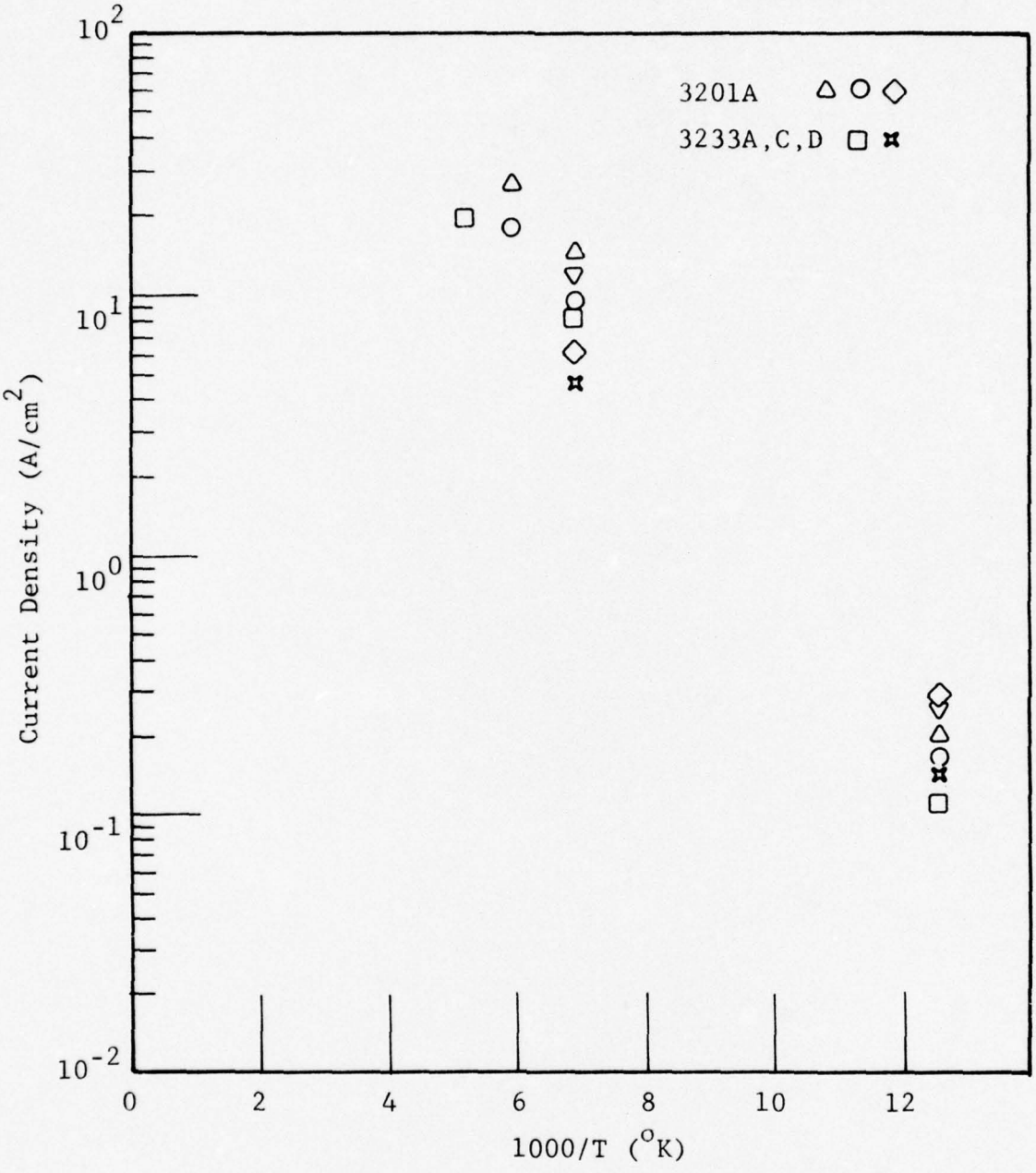

Figure 3.1 SATURATION CURRENT DENSITY VS TEMPERATURE

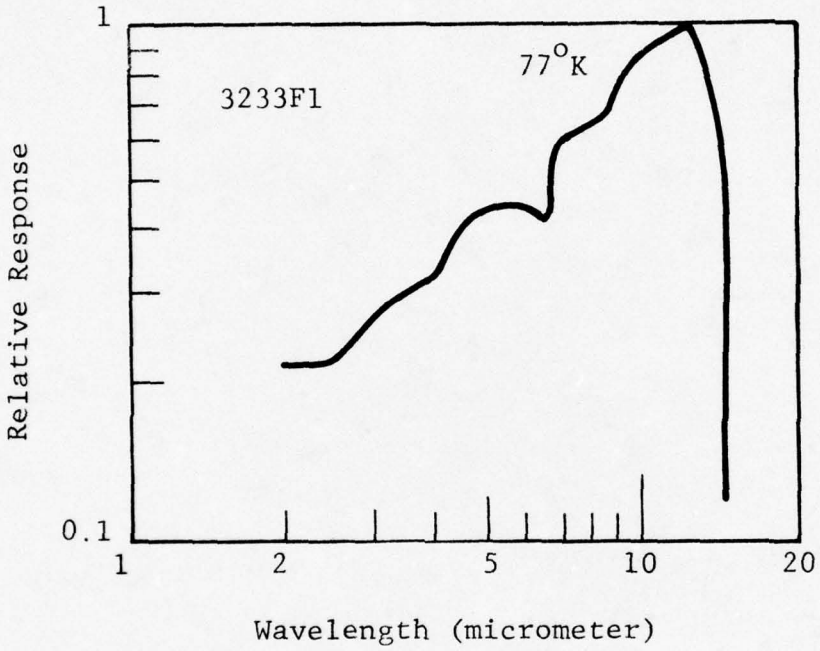

Figure 3.2 SPECTRAL RESPONSE

With 10^{-4} torr vacuum, the cooler achieved 180°K; with 2×10^{-6} torr vacuum, the cooler reached 174°K. Cooldown time to operating temperature was 3 minutes and 20 seconds. Approximately 19 watts are required for operation. Figure 3.3 shows the 6-stage TE cooler. Figure 3.4 shows the assembled module with heat exchanger.

3.2.2 Detectors

Detectors were checked by measuring current density and blackbody responsivity. Table 3.3 summarizes these results. Heterodyne measurements were made at Honeywell Systems and Research Center by Dr. Hans Mocker.

The Appendix contains a detailed report of his measurements. The bandwidth on unit G1 was not measurable because of a low signal-to-noise ratio. Blackbody signal measurements were also impossible because of low signal-to-noise ratio.

Figure 3.5 shows the reverse current characteristic of detector F1 at 173°K during testing. Figure 3.6 shows the forward and reverse current of detector G1 as a function of voltage.

Table 3.3

MODULE PERFORMANCE

	Units	Unit No. 1 (Detector F1)	Unit No. 2 (Detector G1)
Temperature	°K	173	174
J_{SAT}	A/cm^2	48.2	88.9
R_{BB} (4 kHz)	A/W	2.23	NM
R_λ	A/W	4.65	NM
η_λ peak	---	51%	NM
$\eta_{10.6\ \mu m}$	---	26%	NM
Heterodyne MDP	W/Hz	7.7×10^{-19}	4.0×10^{-17}
Bandwidth	MHz	23	NM

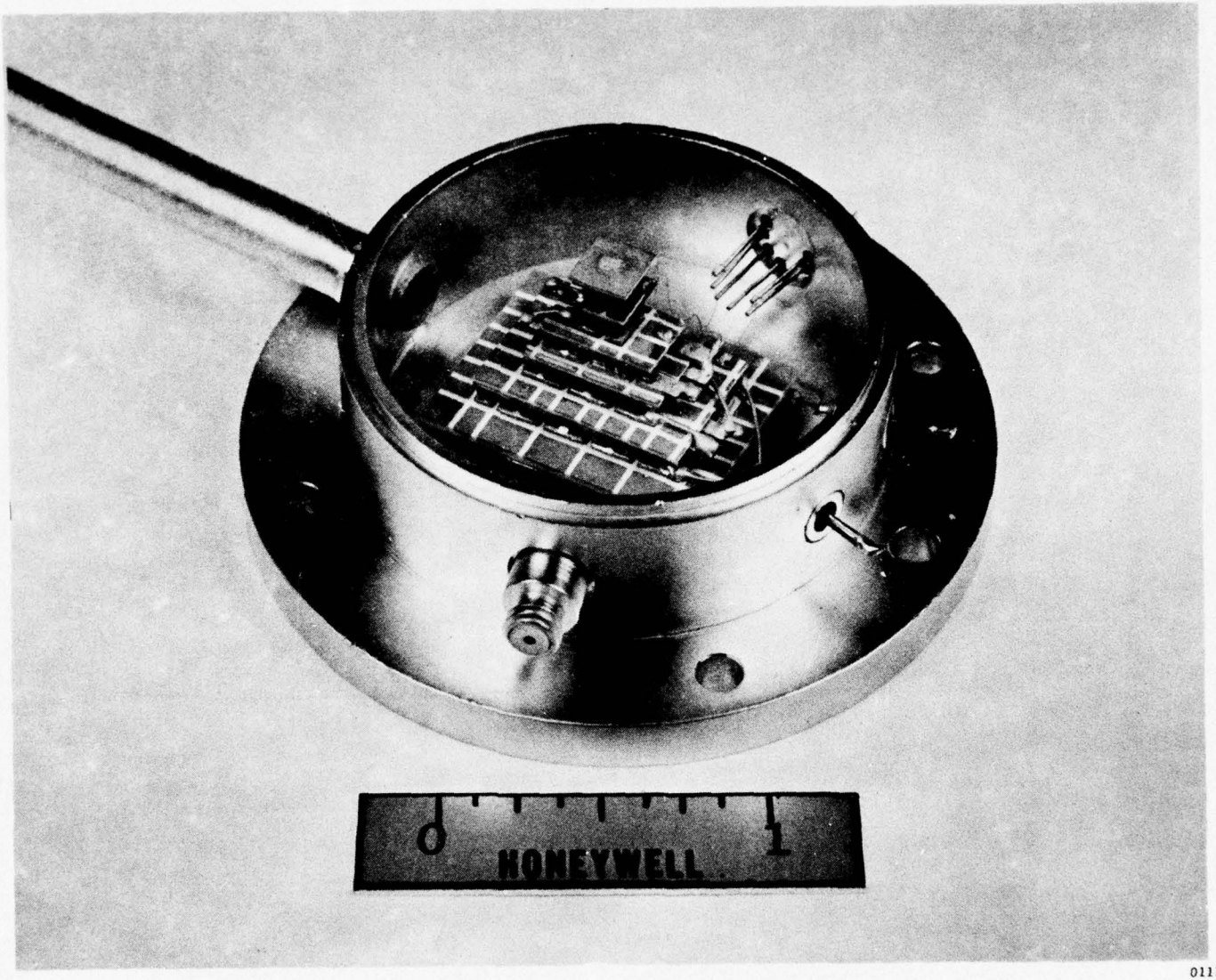

Figure 3.3 THERMOELECTRIC COOLER

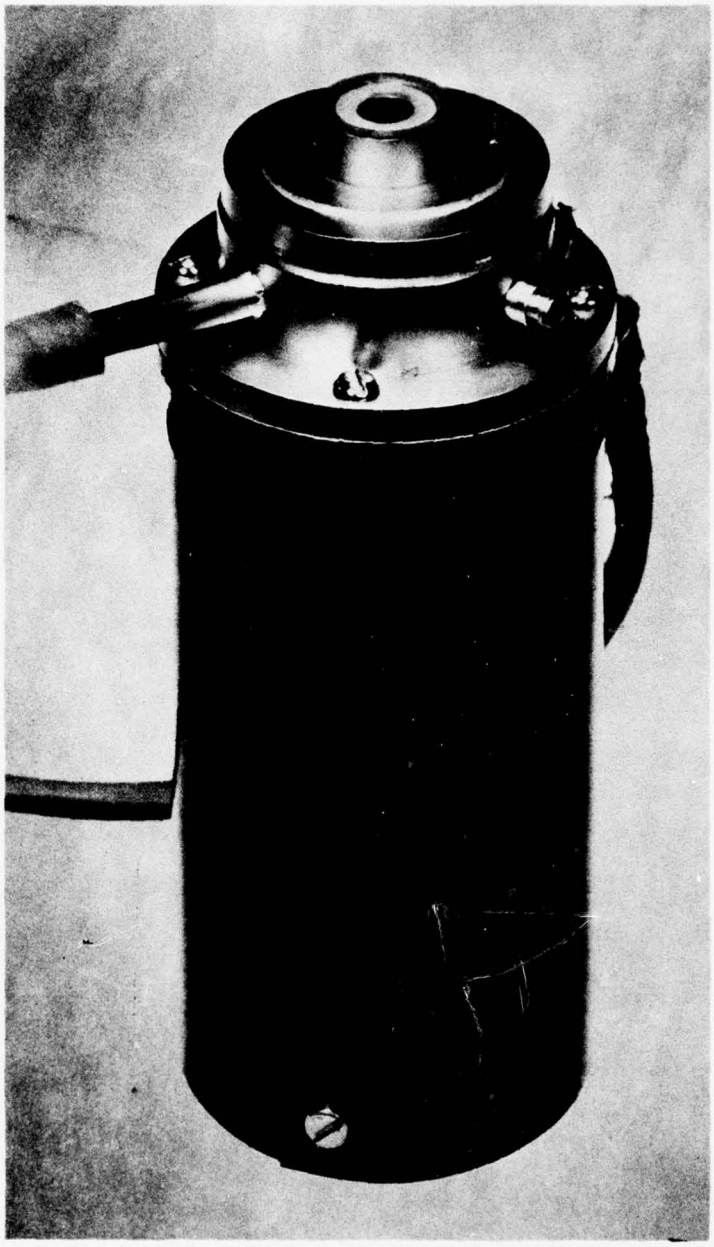

01251

Figure 3.4 ASSEMBLED MODULE WITH HEAT EXCHANGER

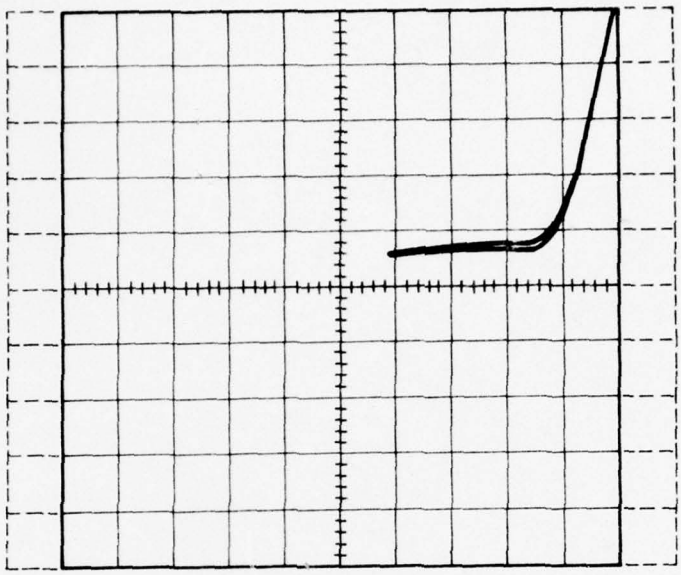

Figure 3.5 REVERSE CURRENT VS VOLTAGE OF DETECTOR F1 AT 173^{o}K

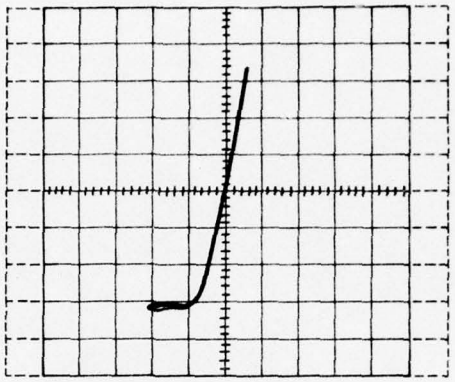

Vertical
5 mA /division

Horizontal
200 mV /division

Figure 3.6 FORWARD AND REVERSE CURRENT OF DETECTOR G1 AS A FUNCTION OF VOLTAGE

3.3 DISCUSSION

The simple model presented in Section 2 and used in the initial phase of this program, assumed a constant mobility to lifetime ratio in the diffusion current equation. This assumption focused our approach on producing a heavily doped junction for 170°K operation. During the program we expanded the model to include temperature dependence of mobilities and lifetimes and examine the consequences on our approach. At the same time, we examined some of the experimental findings in this extended theoretical framework. The major experimental observations were that current density does decrease with doping, quantum efficiency increases with temperature, and bandwidth is diffusion limited by a time constant much longer than one would expect for p-type material at 77°K which has a 1-ns electron lifetime.

3.3.1 Extended Model

The only changes made in the model are: (1) electron mobility, (2) hole mobility, and (3) lifetimes are functions of temperature. The lifetime functions are based on a paper by Kinch.[5] The hole lifetime (τ_h) on the n-side is assumed Auger limited. Above 170°K, τ_h is intrinsic Auger; i.e., independent of doping. The p-side electron lifetime (τ_e) is assumed to be radiative. These lifetimes are expressed as:

$$\tau_h = \tau_{Ai} \left(2ni^2/N_D^2\right)$$

where

$$\tau_{Ai} = 7.6 \times 10^{-18} \, e_\infty^2 \, (1+\mu)^{\frac{1}{2}} \, (1+2\mu)$$

$$\times \exp \left\{ \left[(1+2\mu)/(1+\mu)\right] \, Eg/kT \right\}$$

$$\times \left[(m_e^*/m_o) \, |F_1 F_2|^2 \left(\frac{kT}{qEg}\right)^{3/2} \right]^{-1}$$

and

$$\tau_e = 1/(B * N_A)$$

where

$$B = 5.8 \times 10^{-13} \, e_\infty^{\frac{1}{2}} \left(\frac{m_o}{m_e^* + m_h^*}\right)^{3/2} \left(1 + \frac{m_o}{m_e^*} + \frac{m_o}{m_h^*}\right)$$

$$\times \left(\frac{300}{T}\right)^{3/2} \, Eg^2$$

The value for the overlap integral F_1F_2 is selected as 0.5 to give the best agreement with the calculation by Buss in the paper by Kinch, et al.

Other parameters are:

$$e_\infty = 12.5\ \varepsilon_o$$

$$m_e^* = 0.005$$

$$m_h^* = 0.55$$

$$n_i = (8.46-2.29\ x + 0.00342T)(10^{14}\ Eg^{.75})$$
$$x\ (T^{1.5}\ \exp\ (-Eg/2kT)$$

The minority carrier mobility is based on expression fit to experimental data by S. Tobin.[9] The minority carrier mobilities are calculated by assuming a constant mobility ratio (μ_e/μ_h) of 150. The electron mobility in p-type (Hg,Cd)Te is expressed as:

$$\mu_e = 1.2 \times 10^5/T^{0.4}$$

The hole mobility in n-type (Hg,Cd)Te is expressed as:

$$\mu_h = 3.3 \times 10^7/T^{2.3}$$

Figure 3.7 shows the diffusion current density based on this model as a function of donor concentration and acceptor concentration at 170°K. The model indicates that if the p-side lifetime is radiative, then the current density is determined by the n-side diffusion. At concentrations less than 10^{16} cm^{-3}, the hole lifetime is intrinsic Auger and diffusion current can be lowered by doping the n-side to higher concentrations. Above 10^{16} cm^{-3}, the current density cannot be improved by either p-side doping or n-side doping. This effect is a consequence of hole Auger lifetime, becoming a function of doping and cancelling any effects on diffusion current. The current is still determined by the n-side diffusion. The value of 10 A/cm^2 represents a limit to current density at 170°K.

The n-side doping concentrations of less than 7.9×10^{15} cm^3 at 170°K, can be neglected because junctions will not occur below the intrinsic concentration of 11-μm cutoff wavelength material. It can be assumed that junctions that are observed have concentrations higher than this.

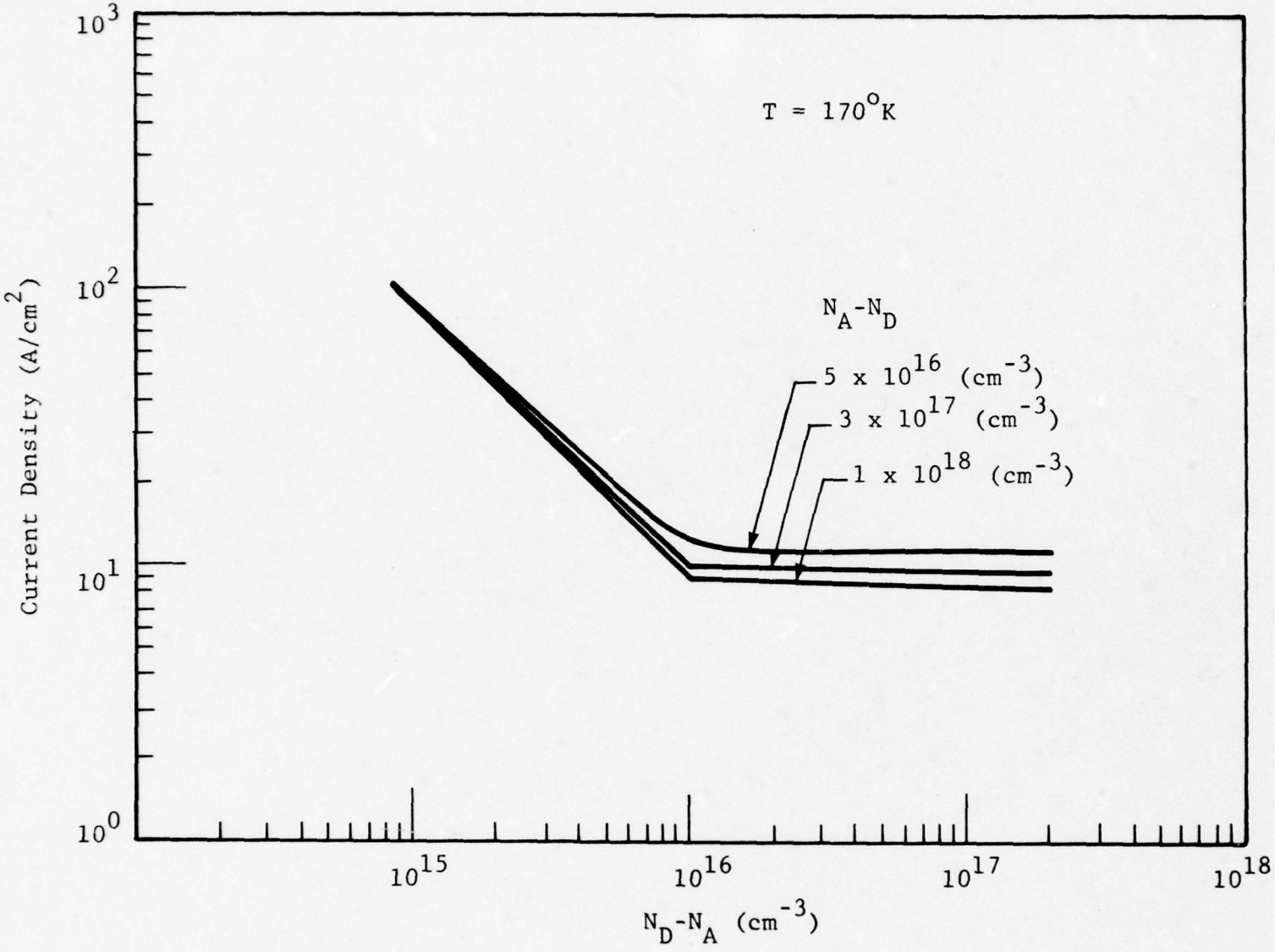

Figure 3.7 CALCULATED CURRENT DENSITY AS A FUNCTION OF JUNCTION DOPING

Experimental results, however, show detector F1 has a current density of 37 A/cm^2 and a 6.9-ns response time. This current density and response are not possible with the n-side limited model. One explanation would be that the p-side electron lifetime is not radiative. Figure 3.8 shows calculations of the current density at 170°K as a function of τ_e for a concentration of 5×10^{16} cm^3 and 3×10^{17} cm^3. The limits for various n-side concentrations are also shown. If the detectors had radiative electron lifetime they would be diffusion limited by the n-side.

Detector F1 was fabricated in 6×10^{16} cm^{-3} p-type material and therefore, fits this model very well. The figure suggests it may be possible to achieve a wider bandwidth and improved current density with a more heavily doped p-side. Detector batch 3201 was fabricated in 2×10^{17} cm^{-3} p-type material and had a current density in the range 18 to 26 A/cm^2 at 170°K. Figure 3.8 predicts a 1-ns response time or a 156 MHz bandwidth for these detectors.

Lifetimes of this magnitude are observed in 77°K (Hg,Cd)Te photodiodes and are attributed to a Schockly-Read recombination centers in p-type material. The center has been hypothesized to be a defect, and therefore, the decrease of lifetime would be consistent with increased doping, i.e., defect concentration.

The model also predicts that the optically active region in this case would be the p-side. A 1×10^{-9} s lifetime produces a 4.7-μm diffusion length which is adequate for high quantum efficiency if the junction is shallow and/or the n-layer is degenerate.

It should be noted that the bandwidth is not RC limited in detector 3233F1. The p-side concentration was measured as 6×10^{16} cm^{-3}. With 0.1 volt bias, 8.3 ohm series resistance and 2×10^{-4} cm^2 area, the capacitance is 57.6 pF. With a 50 ohm amplifier, this is equivalent to 47 MHz. The actual bandwidth is probably higher because the n-side concentration is less than 6×10^{16} cm^{-3}.

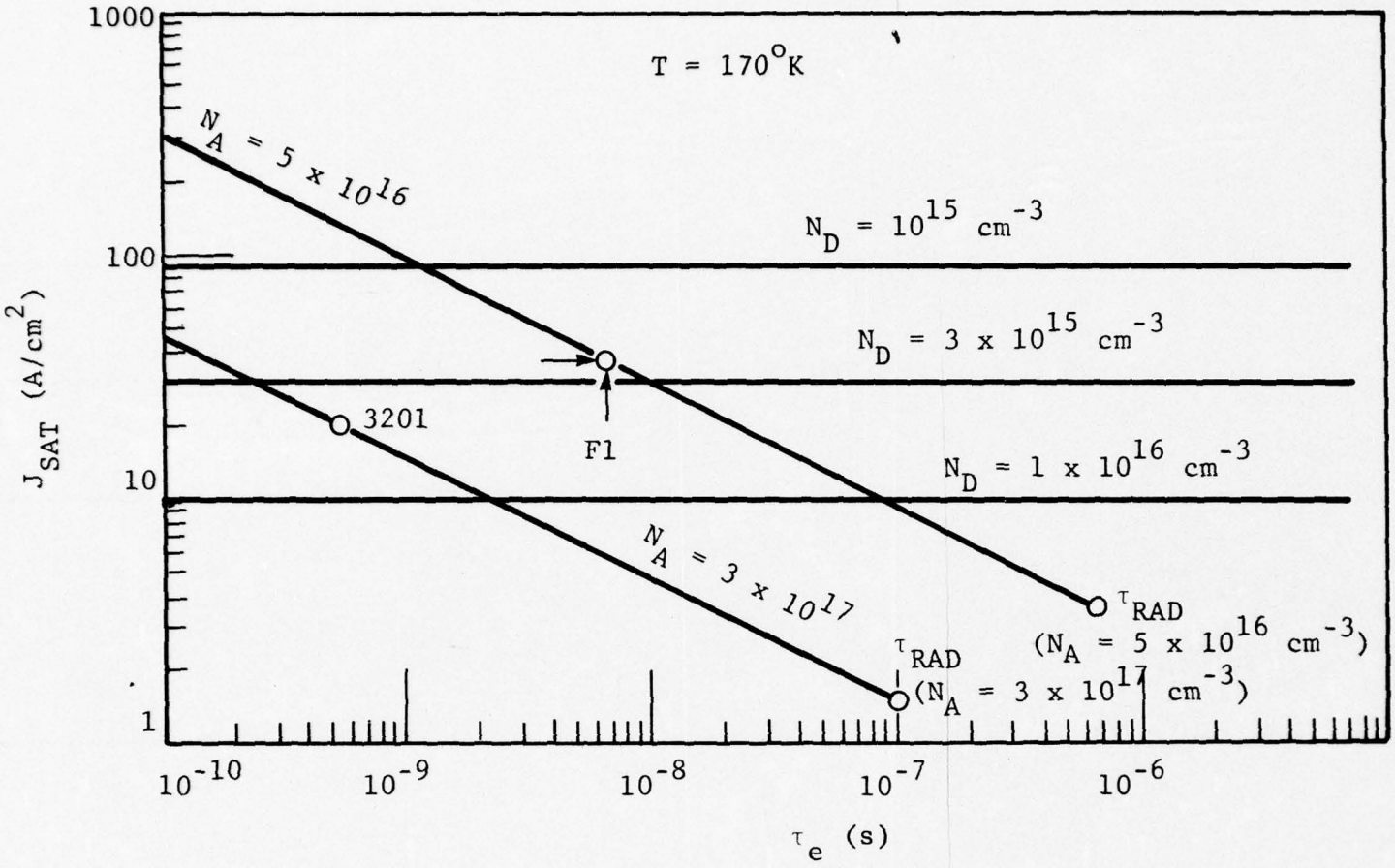

Figure 3.8 CURRENT DENSITY AS A FUNCTION OF P-SIDE MINORITY CARRIER LIFETIME

SECTION 4

CONCLUSIONS AND RECOMMENDATIONS

As a result of this program, the following conclusions can be made about 10.6-μm (Hg,Cd)Te photovoltaic photomixers cooled to 170°K by thermoelectric coolers;

1. Operation at 170°K was demonstrated with 7.7×10^{-19} W/Hz minimum detectable power and 23 MHz bandwidth.

2. The theoretical diffusion current density limit with Auger hole lifetime on the n-side and radiative electron lifetime on the p-side is 10 A/cm^2. In a 250-μm diameter device, this is equivalent to 5 mA. Therefore, the design goal of 1 mA is not realizable in this size. A 150-μm diameter device would have a 2 mA diffusion current which can be dominated by a local oscillator current.

3. In the present devices, the radiative lifetime is not observed in p-type material. A lifetime of 6.9 ns is observed and is assumed to be related to defect related to the acceptor concentration. The observed current densities of 20 A/cm^2 and 44 A/cm^2 at 170°K are consistent with this doping and lifetime. Improvements in present devices can be made by increasing the p-type concentration. Such improvement would ultimately be limited to 10 A/cm^2 by the n-side diffusion current.

4. High diffusion current does not necessarily degrade mixer performance, especially if the thermoelectric cooler can handle 10^{-2} watts of power dissipation.

5. Techniques for achieving junctions with 3×10^{18} cm^{-3} acceptor concentration were not demonstrated. The quench technique only achieved 5×10^{17} cm^{-3} concentration. Copper doping achieved 3×10^{18} cm^{-3} concentration, but conventional indium doping techniques failed to produce an n-layer, i.e., a junction.

The devices delivered were fabricated in 6×10^{16} cm^{-3} p-type material with 6.9 ns minority carrier lifetime at 170°K. It is believed that this lifetime can be reduced to 1 ns in

3×10^{17} cm^{-3} material. This type of device would permit greater than 50 MHz bandwidth operation. It is recommended that devices of this type should be demonstrated experimentally.

The size goal of 250-μm diameter is not feasible because of a 10 A/cm^2 diffusion current limit at 170°K. Future devices should be restricted to 150-μm diameter or less.

The program has devoted no effort to thermal stability. Encapsulation techniques are available and should be applied to future devices to permit bakeout of detector and thermoelectric cooler to achieve long vacuum life for the module.

SECTION 5

REFERENCES

1. R. J. Keyes and T. M. Quist, Semi-conductors and Semi-metals, Vol. 5, 321, 1970.

2. M. C. Teich, "Coherent Detection in the Infrared," Semi-conductors and Semi-metals, Vol. 5, Chapter 9, 1970.

3. B. J. Peyton, et al, IEEE J. Quantum Electronics, Vol. QE-8, No. 2, February 1972.

4. T. Koehler and P. J. McNally, Optical Engineering, July/Aug 1974.

5. M. A. Kinch, M. J. Brau, and A. Simmons, J. Applied Phys., Vol. 44, No. 4, April 1973.

6. C. Burke and T. Koehler, sixth DOD Laser Conference, March 1974.

7. H. Mocker and T. Koehler, "Miniaturized Coherent Transmitter-Receiver System," Proc. Electro-Optical Systems Conference, 593, November 1975.

8. D. L. Spears, IRIS Detector Specialty Group Meeting, Washington, DC, March 1973.

9. S. Tobin (Private Communication).

APPENDIX

HETERODYNE CHARACTERIZATION OF TWO TE-COOLED (Hg,Cd)Te PHOTOMIXERS

by
Dr. Hans Mocker

This Appendix summarizes the results of measurements on two (2) thermoelectrically-cooled (Hg,Cd)Te Detector Modules, Type LK 170 A1., Serial Nos. U1-K1 (referred to as Unit 1) and U2-K1 (referred to as Unit 2). Unit 1 contains detector F1 and Unit 2 contains detector G1. These measurements were carried out at the Honeywell Systems and Research Center.

Eight different types of measurements were made on Unit 1. Unit 2 was only investigated for 1 to 3 due to its higher dark current and lower NEP. The following measurements were made on Detector U1-K1:

1. Current-voltage diagram (also for Unit 2) with local oscillator power parameter.
2. Derived from 1: sensitivity to 1. o. power induced current vs 1. o. power (also for Unit 2)
3. Determination of NEP (also for Unit 2)
4. Determination of S/N-ratio as a function of 1. o. power for 5 different bias conditions.
5. Determination of current-voltage characteristics as a function of 1. o. power (for 5 different bias conditions).
6. Determination of detector temperature as a function of 1. o. power for 5 bias conditions.
7. Noise investigations from motor.
8. Frequency response measurement (0-30 MHz).

I. DESCRIPTION OF THE EXPERIMENTAL SETUP

For the reported measurements the following experimental setup was used (the schematic is shown in Figure 1). Two stable Honeywell CO_2 lasers (Models 3000 and 7000) with a power output of 3 watts and 8 watts, respectively, were used. Both lasers heterodyned have a short-term stability of better than 10^9 and a long-term stability of better than 10^7. The model 7000 was designated as local oscillator (1. o.) and its power level coarse - attenuated by a double - Brewster plate attenuator and fine attenuated by CaF_2 - flats. The 1. o. beam enters through a beamsplitter and is focused by a germanium field lens on the (Hg,Cd)Te detector. The field lens has a focal length of 1.5 inches. The model 3000 is designated to generate variable signal powers. The laser beam can enter through a

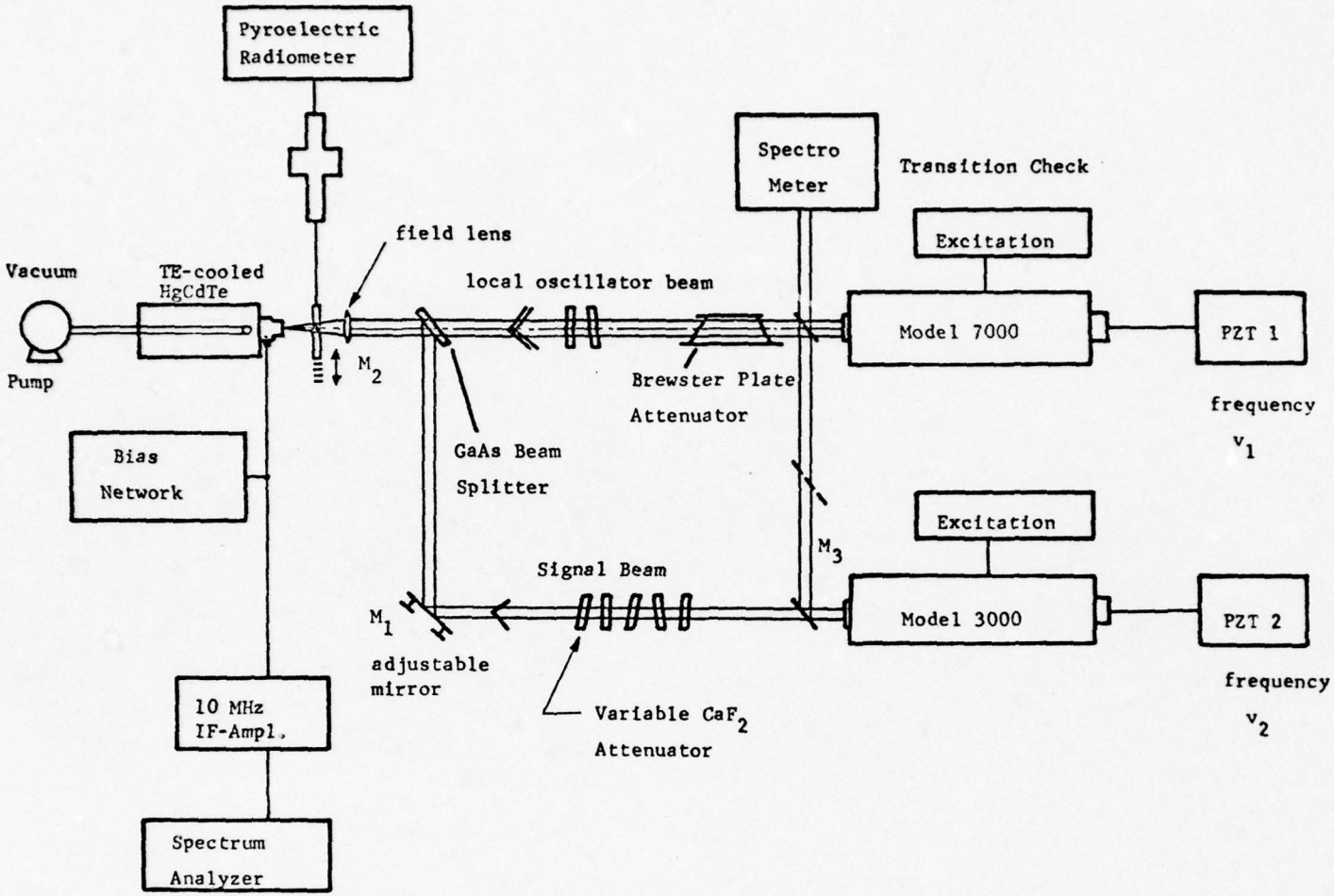

Figure 1 EXPERIMENTAL SETUP FOR SIGNAL-TO-NOISE RATIO MEASUREMENT IN HETERODYNE MODE OF OPERATION

series of optical CaF_2 - flat and an optical attenuation up to 100 dB can be generated in this way. The beam is then reflected on a two-dimensionally adjustable mirror and is then combined with the 1. o. - beam at the germanium beamsplitter. Both beams thus fall spatially coincident on the mercury cadmium telluride detector which is mounted on a two-dimensional positioner.

Beam alignment is accomplished in the following way: the 1. o. beam is chopped by a low-frequency chopper and the two-dimensional positioner of the detector adjusted to obtain maximum signal from the detector. The detector can also be moved along the optic axis for a one-time positioning at the focal point of the field lens. The signal laser beam is then superimposed by adjusting the reflecting mirror M_1 with the signal laser beam being chopped. Fine adjustments are being made once the beat signal of the two lasers has been obtained by maximizing the S/N ratio on the spectrum analyzer.

The power level of the lasers that falls on the detector can be measured by sliding into position a mirror M_2 that reflects the laser energy onto a pyroelectric radiometer (Laser Precision MORK 3440). The transition under oscillation can be adjusted by means of piezoelectric frequency control on each of the lasers and monitored by a Wavelength Analyzer (Optical Engineering) after insertion of a mirror M_3.

Attenuation of the signal laser beam is accomplished by insertion of pairs of calcium fluoride flats that are polished flat to better than $\lambda/10$ and parallel to less than 10 arc seconds. Individual slabs are tilted by 7 degrees with respect to each other to avoid a Fabry-Perot interferometer effect and not to create any lateral beam offset. Each attenuation pair has an attenuation of approximately 10 dB. An independent exact calibration with a CO_2 laser beam was made of each attenuator set.

The detector is evacuated by a 50-liter ion pump to a vacuum of better than 10^{-6} Torr. A bias network as shown in Figure 2 was built to allow the setting of the dc voltage and current applied to the detector. The temperature of the detector is monitored with a thermistor and a digital ohmmeter. A calibration of the device is shown in Table 1.

The output of the detector is fed into an IF amplifier with a center frequency of 10 MHz and a bandwidth of 2 MHz (type RHG 1002). Both lasers are set off to a 10 MHz beat frequency by means of piezoelectric frequency control. Due to their good long-term stability, the lasers will hold the 10 MHz beat frequency over many hours. The output of the IF amplifier is fed into a

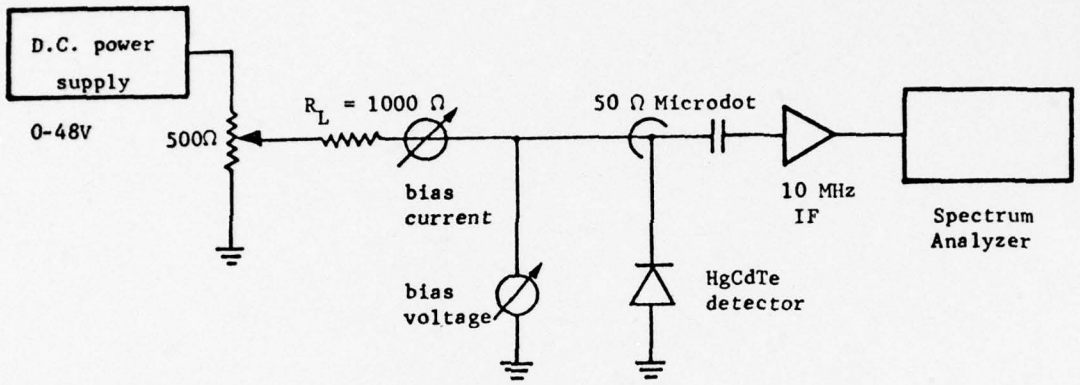

Figure 2 BIAS ARRANGEMENT FOR DETECTOR TESTS

Table 1

HOT SIDE		COLD SIDE	
TEMPERATURE (CELSIUS)	RESISTANCE (K-OHMS)	TEMPERATURE (CELSIUS)	RESISTANCE (K-OHMS)
0.00	3.820	-110.00	3641.757
1.00	3.670	-109.00	3305.013
2.00	3.526	-108.00	3002.936
3.00	3.388	-107.00	2731.621
4.00	3.257	-106.00	2487.640
5.00	3.132	-105.00	2267.975
6.00	3.013	-104.00	2069.970
7.00	2.899	-103.00	1891.284
8.00	2.790	-102.00	1729.848
9.00	2.686	-101.00	1583.834
10.00	2.586	-100.00	1451.624
11.00	2.491	-99.00	1331.784
12.00	2.400	-98.00	1223.041
13.00	2.313	-97.00	1124.265
14.00	2.229	-96.00	1034.450
15.00	2.150	-95.00	952.701
16.00	2.073	-94.00	878.220
17.00	2.000	-93.00	810.295
18.00	1.930	-92.00	748.288
19.00	1.863	-91.00	691.631
20.00	1.798	-90.00	639.814
21.00	1.736	-89.00	592.381
22.00	1.677	-88.00	548.921
23.00	1.620	-87.00	509.066
24.00	1.565	-86.00	472.486
25.00	1.513	-85.00	438.832
26.00	1.463	-84.00	407.987
27.00	1.414	-83.00	379.558
28.00	1.368	-82.00	353.377
29.00	1.323	-81.00	329.247
30.00	1.280	-80.00	306.990
31.00	1.239	-79.00	286.444
32.00	1.200	-78.00	267.463
33.00	1.161	-77.00	249.914
34.00	1.125	-76.00	233.678
35.00	1.089	-75.00	218.645
36.00	1.056	-74.00	204.716
37.00	1.023	-73.00	191.800
38.00	0.991	-72.00	179.816
39.00	0.961	-71.00	168.689
40.00	0.932	-70.00	158.349
41.00	0.904	-69.00	148.736
42.00	0.877	-68.00	139.791
43.00	0.850	-67.00	131.464
44.00	0.825	-66.00	123.706
45.00	0.801	-65.00	116.474
46.00	0.777	-64.00	109.728
47.00	0.755	-63.00	103.431
48.00	0.733	-62.00	97.551
49.00	0.712	-61.00	92.055
50.00	0.692	-60.00	86.917

spectrum analyzer. Both a Hewlett-Packard analyzer (type 8555A) for the frequency response measurements as well as Panoramic analyzer (type SPA-3) have been used.

II. EXPERIMENTAL RESULTS

a) Current-Voltage Diagram.

The current-voltage diagram for Unit 1 (Detector F1) is shown in Figure 3. The detector saturates with no local oscillator power at about 7 mA. (See also Figure 4a) The saturation curve has a fairly flat shoulder but at a higher bias voltage the current starts increasing again at a moderate slope. With increasing local oscillator power the detector increases its saturation level due to the local oscillator induced current. This increase (see Figure 5 and 4b) is initially linear with local oscillator power (up to 3 mW) and starts then to saturate. The slope for detector F1 is 0.8 mA/mW.

The current-voltage diagram for Unit 2 (Detector G1) is shown in Figure 6. This detector never reaches a flat saturation plateau but only signs of onset of saturation and this at substantially higher current levels (12-13 mA). The local oscillator induced current is shown in Figure 7. It shows basically the same behavior as for detector 1 with the exception of a higher slope of 1.6 mA/mW and a reduced linear regime (<1.5 mW). From a comparison of both detectors it appears that the relative local oscillator induced current is approximately identical for both detectors.

b) S/N-Ratio Measurements.

S/N ratio measurements were made with the experimental setup as described in Figure 1. For this purpose a 10 MHz offset frequency was chosen and the effective bandwidth of the receiving system (Panoramic spectrum analyzer) was 130 kHz; the noise figure of the IF-amplifier was 4 dB. Under these conditions the minimum detectable power level for detector F1 was $Ps^{min} = 2.54 \times 10^{-13}$ watts for detector G1 was $Ps^{min} = 1.3 \times 10^{-11}$ watts. Thus, the NEP for detector F1 is $NEP_1 = 7.7 \times 10^{-19}$ W/Hz and for detector G1 $NEP_2 = 4.0 \times 10^{-17}$ W/Hz.

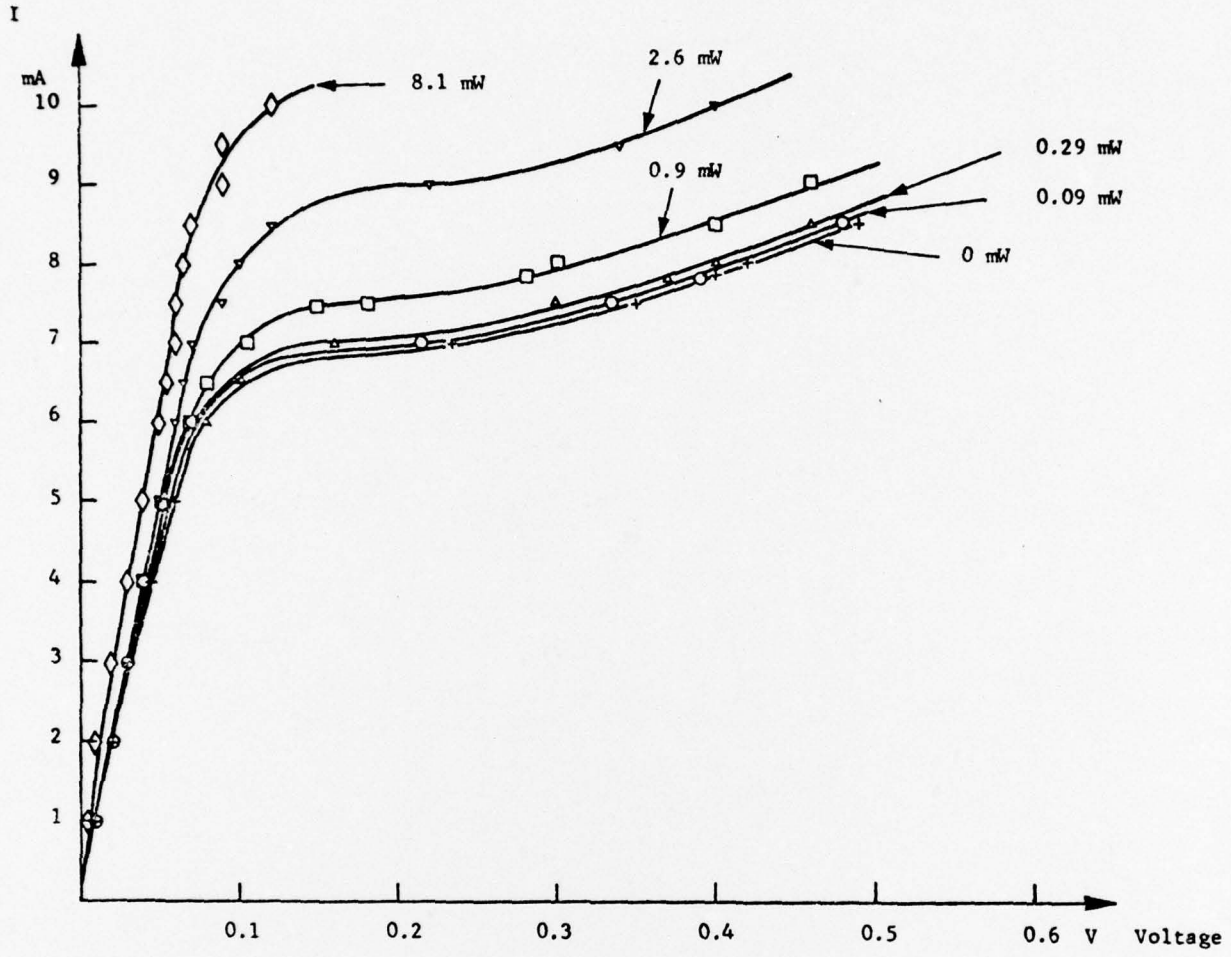

Figure 3 I-V DIAGRAM FOR DETECTOR F1 IN UNIT 1

(a) NO LOCAL OSCILLATOR
POWER APPLIED

(b) WITH AND WITHOUT LOCAL OSCILLATOR
POWER OF ABOUT 0.8 mW APPLIED

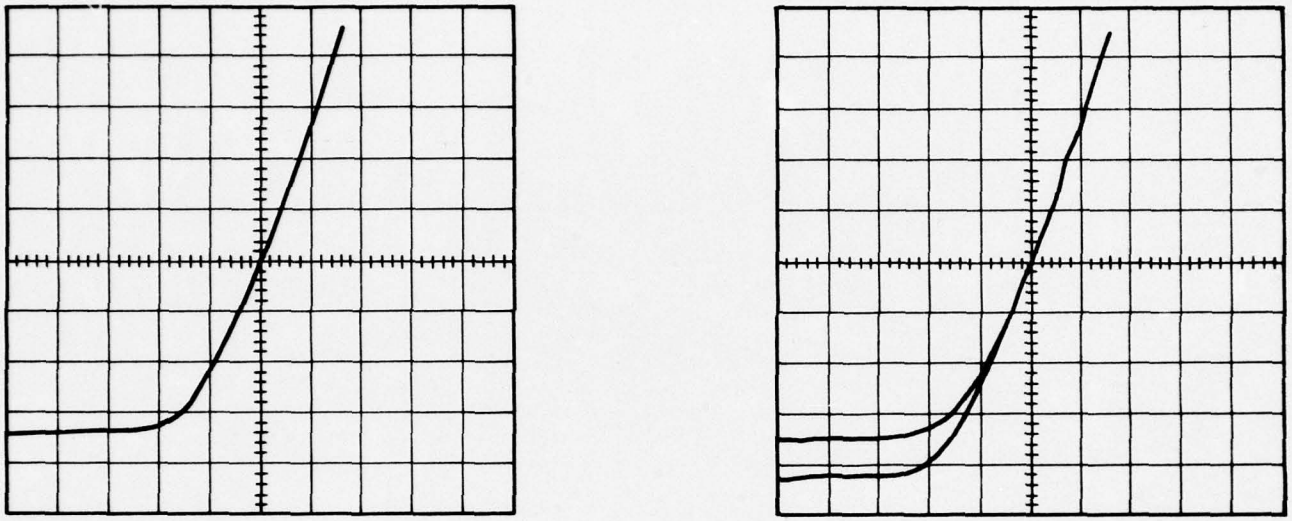

Figure 4 I-V DIAGRAM FOR DETECTOR F1 MEASURED WITH CURVE TRACER

(VERTICAL SCALE: 2 mA/division)
(HORIZONTAL SCALE: 0.5 Volts/division)

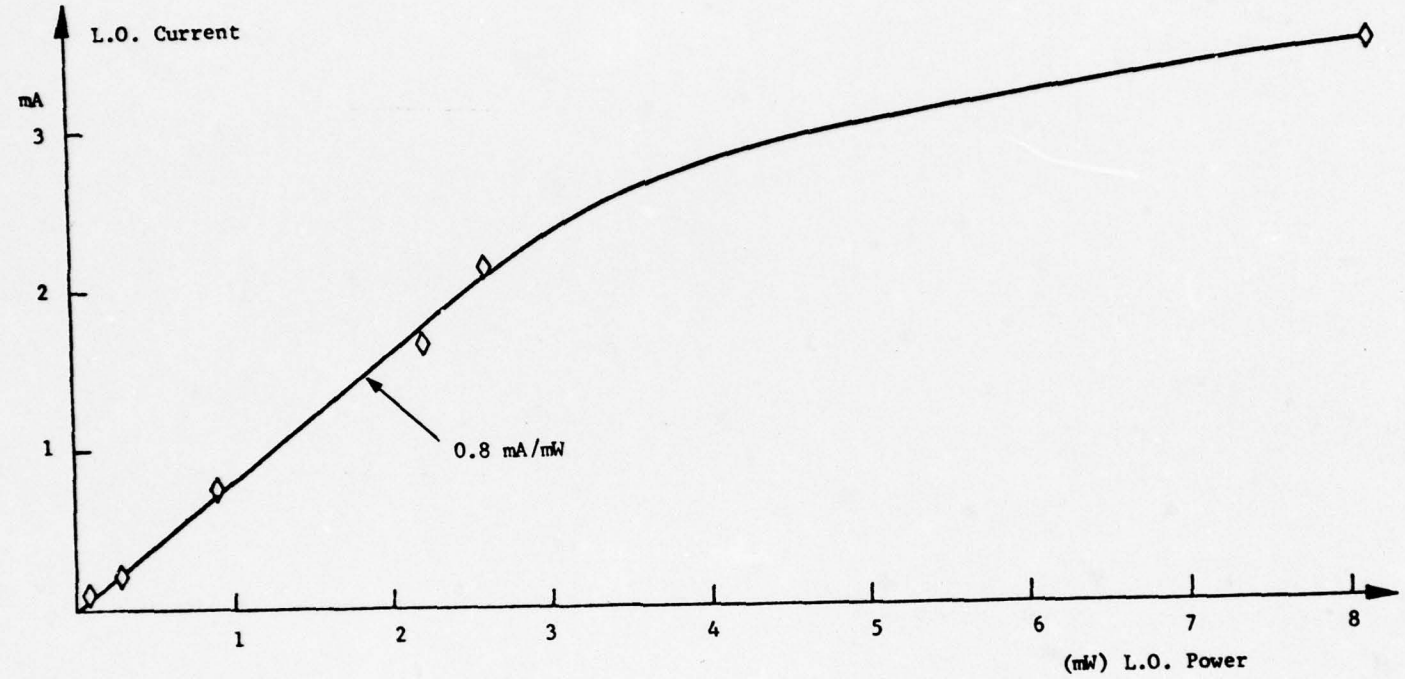

Figure 5 LOCAL OSCILLATOR INDUCED CURRENT VS LOCAL OSCILLATOR POWER FOR DETECTOR F1

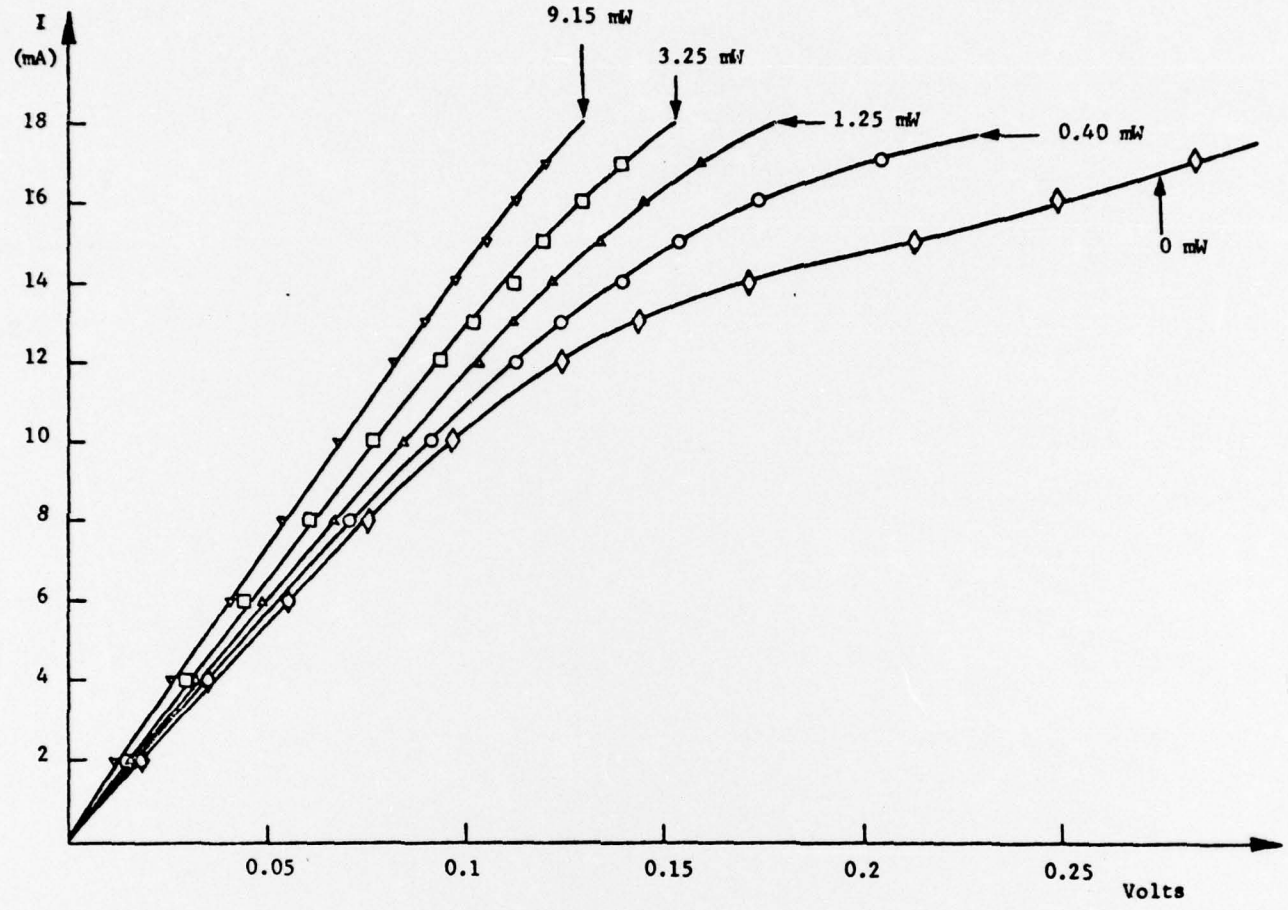

Figure 6 I-V DIAGRAM FOR DETECTOR G1

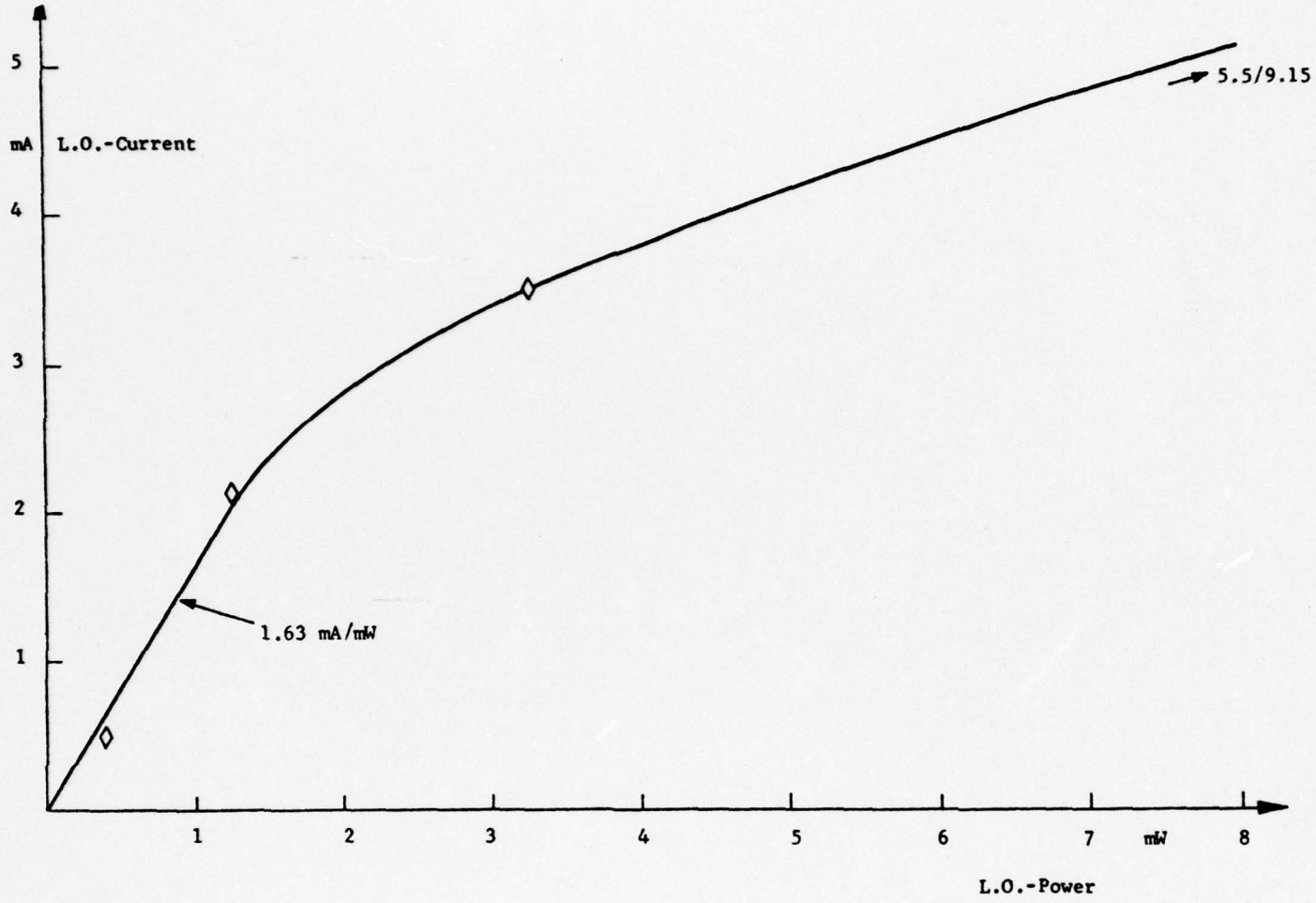

Figure 7 LOCAL OSCILLATOR INDUCED CURRENT VS LOCAL OSCILLATOR POWER FOR DETECTOR G1

c) Local Oscillator Optimization Studies.

For this type of measurement the transmitter laser was attenuated to approximately 10^{-8} watts and the current and voltage values of the detector were determined as the local oscillator level was increased from 0 to 14 mW. The S/N ratio was measured simultaneously on the spectrum analyzer. The initial bias conditions for the detector are shown in Table 2:

Table 2

INITIAL BIAS CONDITIONS FOR DETECTOR F1

Condition	1	2	3	4	5
Current (mA)	6.1	6.7	7.2	7.6	8.3
Voltage (V)	0.016	0.22	0.31	0.387	0.49

Figure 8 shows the change in detector characteristics as a function of local oscillator power. Figure 9 shows the corresponding plot of the S/N ratio as a function of l. o. power. One can see that the S/N ratio is optimized for the bias conditions 4 and 5 and that local oscillation power levels between 0.5 and 1 mW are most suitable for operation. The total dissipated power level for a 1 mW l. o. power and bias condition 4 and 5 is as follows:

Condition 4: 2.1 mW bias + 1 mW l. o. = 3.1 mW total

Condition 5: 3 mW bias + 1 mW l. o. = 4 mW total

Figure 10 shows the temperature of the (Hg,Cd)Te detector as a function of the local oscillator power for the 5 bias conditions as shown in Table 2. Thermal heating of the element becomes noticeable at l. o. power levels of larger than 1 mW. The temperature of the element increases for the bias conditions from 1 through 5 as expected. For the bias conditions 4 and 5 the temperature is reduced for l. o. power levels between 0.5 and 2 mW due to the stronger reduction in bias power. At higher l. o. power levels the temperature increases rapidly due to thermal heating.

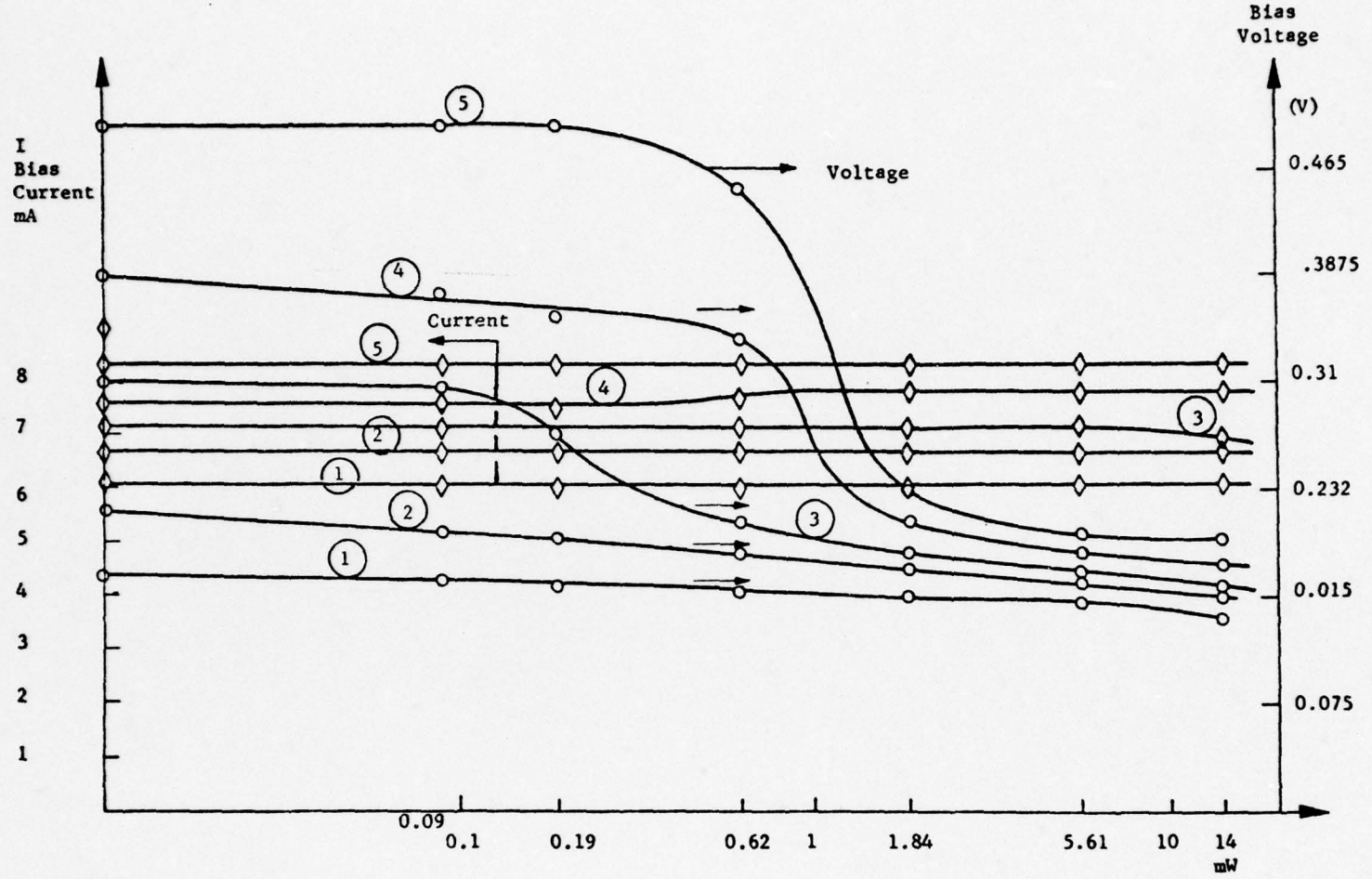

Figure 8 I-V DIAGRAM VERSUS LOCAL OSCILLATOR POWER FOR DETECTOR F1

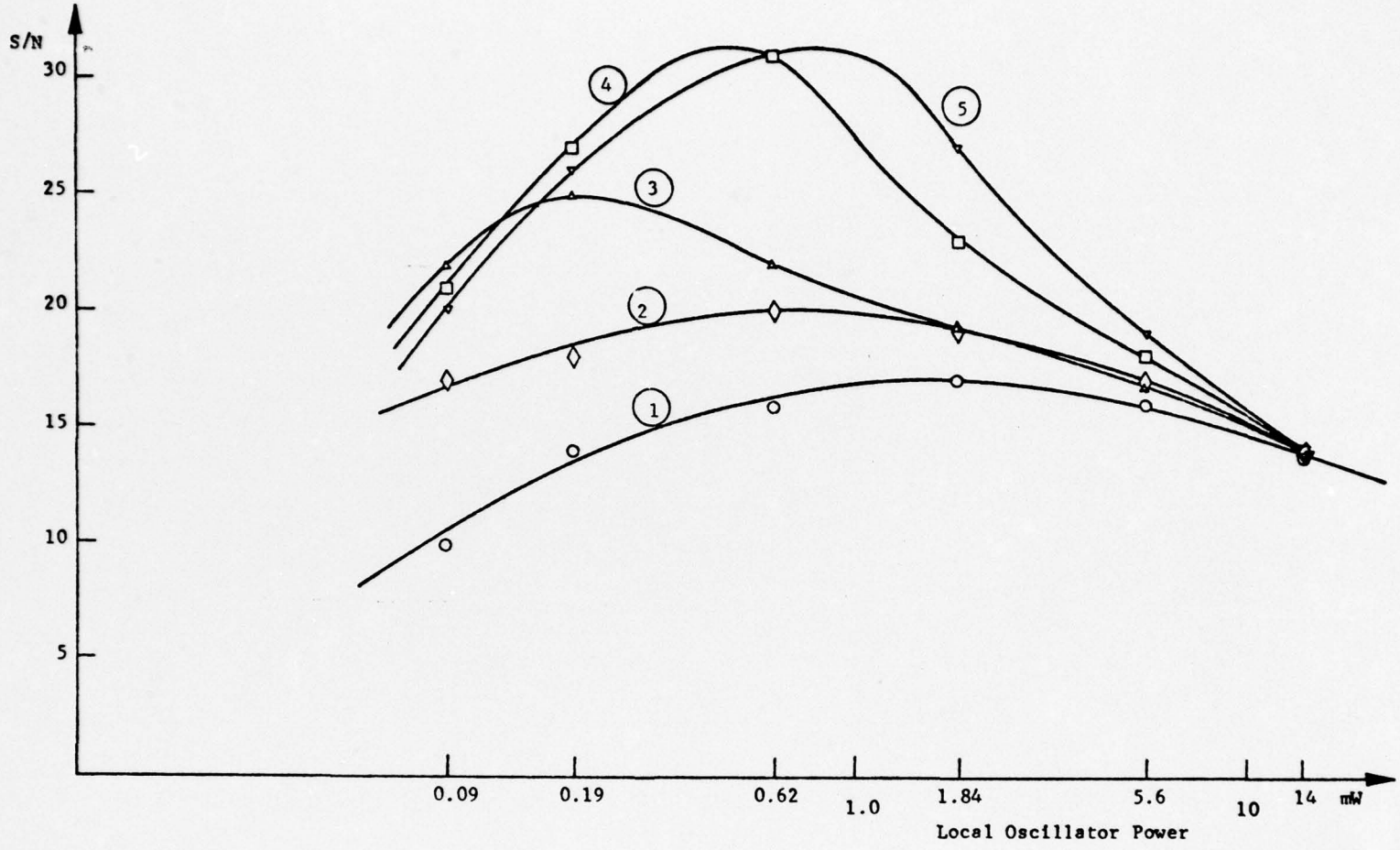

Figure 9 S/N RATIO AS A FUNCTION OF L.O.-POWER FOR VARIOUS BIAS CONDITIONS FOR DETECTOR F1

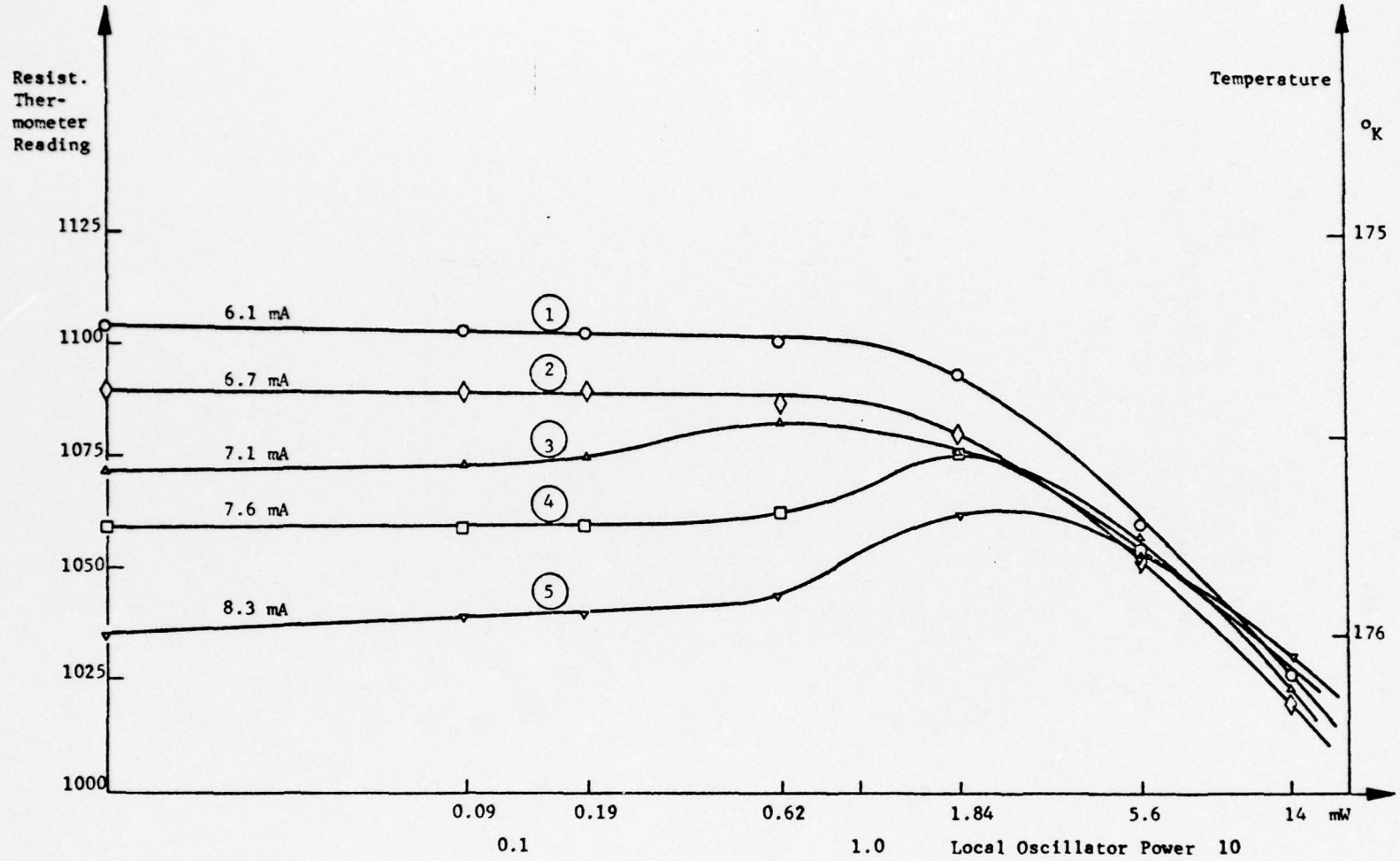

Figure 10 TEMPERATURE OF (Hg,Cd)Te - DETECTOR F1 VERSUS LOCAL OSCILLATOR POWER FOR 5 BIAS CONDITIONS

d) Frequency Response and Motor Noise Determination.

The frequency response of the (Hg,Cd)Te detector was determined by generating a variable offset frequency between 0 and 30 MHz. The S/N ratio over this frequency interval was determined by using the H.P. - spectrum analyzer as a receiver. The result of this measurement for detector F1 is shown in Figure 11. The results indicate that the S/N measurement at 10 MHz did not see any clipping since the response is virtually flat to 20 MHz. The 3-dB rolloff is at 23 MHz.

During measurements with a wideband, low noise amplifier (5-500 MHz, noise figure 2 dB) it was observed that the spectrum seen on the H.P. analyzer showed a multiplicity of noise spikes at discrete but in time slowly varying frequencies. In order to determine their origin and order of magnitude a beat signal of approximately 30 dB was generated at a frequency of 10 MHz and sent into a wideband amplifier and H.P. analyzer. Besides the beat noise at 10 MHz (and a self-beat of the laser at 5 MHz) a large number of noise beats can be seen between 5 and 50 MHz. To confirm that the noise is due to the immediate increase in detector temperature. Thus, it appears that future work should consider shielding the detector or using a pneumatically driven turbine blade for cooling purposes.

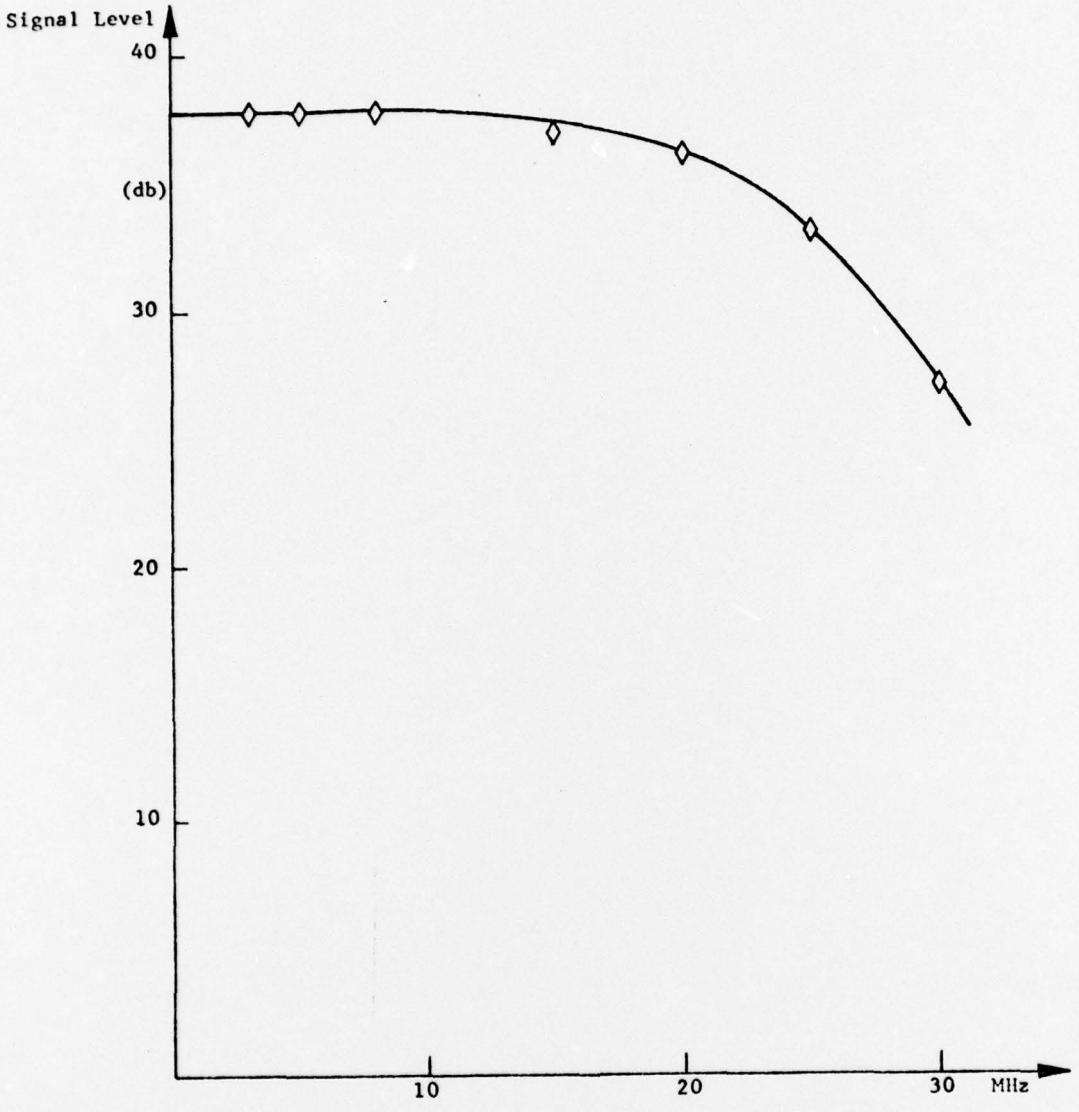

Figure 11 FREQUENCY RESPONSE OF TE-COOLED (Hg,Cd)Te DETECTOR F1

DISTRIBUTION LIST

Defense Documentation Center ATTN: DDC-TCA Cameron Station (Bldg 5) Alexandria, VA 22314		12
Commander US Army Electronics Command Fort Monmouth, NJ 07703		
ATTN:	DRSEL-PP-I-PI	1
	DRSEL-PL-ST	1
	DRSEL-WL-D	1
	DRSEL-VL-D	1
	DRSEL-CT-L-C (Mrs. C. Burke)	8
	DRSEL-BL-D	1
	DRSEL-CT-L (Dr. R.G. Buser)	1
	DRSEL-CT-L-C (Dr. E. Tebo)	1
	DRSEL-CT-L (Mr. B. Louis)	1
	DRSEL-CT-L-D (Dr. E. Schiel)	1
	DRSEL-CT-L-E (Dr. H. Hieslmair)	1
	DRSEL-TL-D	1
	DRSEL-NL-R-5 (Dr. E. Dworkin)	1
	DRSEL-VL-E	1
	DRSEL-WL-N	1
	DRSEL-CT-L (Ofc of record)	1
	DRSEL-MA-MP	1
	DRSEL-MS-TI	1
	DRSEL-GG-TD	1
	DRSEL-PA	1
	AMCPM-TDS-SE	1
	USMC-LNO	1
	DRSEL-RD	1
	TRADOC-LNO	1
	DRSEL-CT-L-B (Mr. R. Tuttle)	1
	DRSEL-GG (Mr. Doxey)	1
Advisory Group on Electron Devices ATTN: Secretary, Working Group D (Lasers) 201 Varick Street New York, NY 10014		2
NASA Scientific & Technical Information Facility ATTN: Acquisitions Branch (S-AK/DL) P.O. Box 33 College Park, MD 20740		1
Commander US Army Armament Command ATTN: DRSAR-RDT (Mr. Robert Seamands) Rock Island, IL 61201		1

DISTRIBUTION LIST (continued)

Commander 1
Naval Electronics Laboratory Center
ATTN: Electro-Optics Division 2500 (Dr. G.C. Mooradian)
San Diego, CA 92152